Tropical tree growth driven by dry-season climate variability

Interannual variability in the global land carbon sink is strongly related to variations in tropical temperature and rainfall. This association suggests an important role for moisture-driven fluctuations in tropical vegetation productivity, but empirical evidence to quantify the responsible ecological processes is missing. Such evidence can be obtained from tree-ring data that quantify variability in a major vegetation productivity component: woody biomass growth. Here we compile a pantropical tree-ring network to show that annual woody biomass growth increases primarily with dry-season precipitation and decreases with dry-season maximum temperature. The strength of these dry-season climate responses varies among sites, as reflected in four robust and distinct climate response groups of tropical tree growth derived from clustering. Using cluster and regression analyses, we find that dry-season climate responses are amplified in regions that are drier, hotter and more climatically variable. These amplification patterns suggest that projected global warming will probably aggravate drought-induced declines in annual tropical vegetation productivity. Our study reveals a previously underappreciated role of dry-season climate variability in driving the dynamics of tropical vegetation productivity and consequently in influencing the land carbon sink.

Tropical and subtropical ecosystems are primarily responsible for the large interannual variability in the global carbon land sink[1-4]. In cooler and wetter years in the tropics, carbon uptake by tropical vegetation is large and increases the global land sink, whereas warmer and drier years reduce this sink[5-7] or flip it into a carbon source[8]. The response of tropical vegetation productivity to variability in moisture availability probably contributes to these emergent global patterns[6]. A better understanding of the global land sink variability therefore requires quantifying the effect of climatic variation on tropical vegetation productivity. Yet, the sensitivity of key components of tropical vegetation productivity, such as woody biomass growth, to climate variability is poorly understood. Direct, long-term and temporally highly resolved measurements of these components are needed to reconstruct[2], simulate[9,10] and forecast the carbon land sink[11,12].

In this Article, we evaluate the climate responses of woody biomass growth throughout the global tropics (here defined as 30°N–30°S, including subtropics). We focus on woody biomass growth in tree stems, which constitutes a significant share of net productivity of tropical vegetation at local[13,14] to continental scales[15,16], contributes to the main long-term carbon reservoir in tropical biomass[17] and determines the success of forest-based natural climate solutions[18]. Using a compilation of tropical tree-ring data, we test three hypotheses on the association between climate and annual woody biomass growth of trees (hereafter, 'tree growth') across tropical climate zones that vary in temperature and precipitation. (1) We expect opposite associations of tree growth with precipitation (positive) and temperature (negative), consistent with those observed for the land sink[5,6]. (2) We expect the magnitude of these associations to peak in the wet season, when photosynthesis[19] and woody biomass growth[20] in tropical vegetation are typically highest. (3) Finally, we expect climate–growth associations to amplify with site aridity because semi-arid regions exhibit stronger climatic variability[1] and contribute more to interannual variability in the land sink[1,3,4,21]. Hereafter, we will refer to associations between climate and tree growth as 'climate responses'.

We established a network of 415 tree-ring chronologies (time series of absolutely dated, population-level average ring width) compiled from tropical and subtropical latitudes (Extended Data Fig. 1). From this network, we selected 347 chronologies that fulfilled

quality criteria of sample size, chronology robustness and length and that covered recent decades. The chronologies are derived from 99 tree species on 5 continents and were obtained from co-authors ($n = 112$ chronologies) and the International Tree-Ring Data Bank (ITRDB; $n = 235$).

To facilitate comparative analyses of tree climate responses across the network, we re-developed standardized ring-width index (RWI) chronologies using a single detrending method. We then assessed climate associations by relating the most recent 50 years of all RWI chronologies to gridded climate data (Extended Data Table 1). We chose to evaluate climate associations with precipitation (PP) and maximum temperature (T_{max}) instead of commonly used drought indices because these climate data are directly measured and available for multiple decades and because T_{max} is a strong driver of tropical woody biomass growth[22].

We tested our first two hypotheses using two complementary approaches. First, to detect common modes of climate response across the network, regardless of biogeographic region, we performed a self-organizing maps (SOMs)[23] cluster analysis based on RWI responses to monthly PP and T_{max} over a 2 yr period during and before the year of ring formation. This approach allows for detecting idiosyncratic and lagged responses of tree growth to monthly climatic conditions[24]. We present the results based on a 2×2 SOM grid, which resulted in four groups of climate response. Second, to evaluate the relative influences of T_{max} and PP on tree growth during the wet (PP > 100 mm month⁻¹) (ref. [25]) and dry (PP < 100 mm month⁻¹, preceding ring formation) seasons, we conducted a multiple linear regression analysis of RWI for each chronology. This more-restrictive analysis included only seasonally significant ($P < 0.05$) and additive effects of the two climatic variables during a 1 yr period. For both approaches, we tested hypothesis 3 by associating climate responses with ambient hydroclimatic conditions.

Network representativeness

Our network covers a large portion of climatic conditions and biomes on tropical land area (Fig. 1a,b and Extended Data Fig. 1). The network is climatologically representative for 66% of the
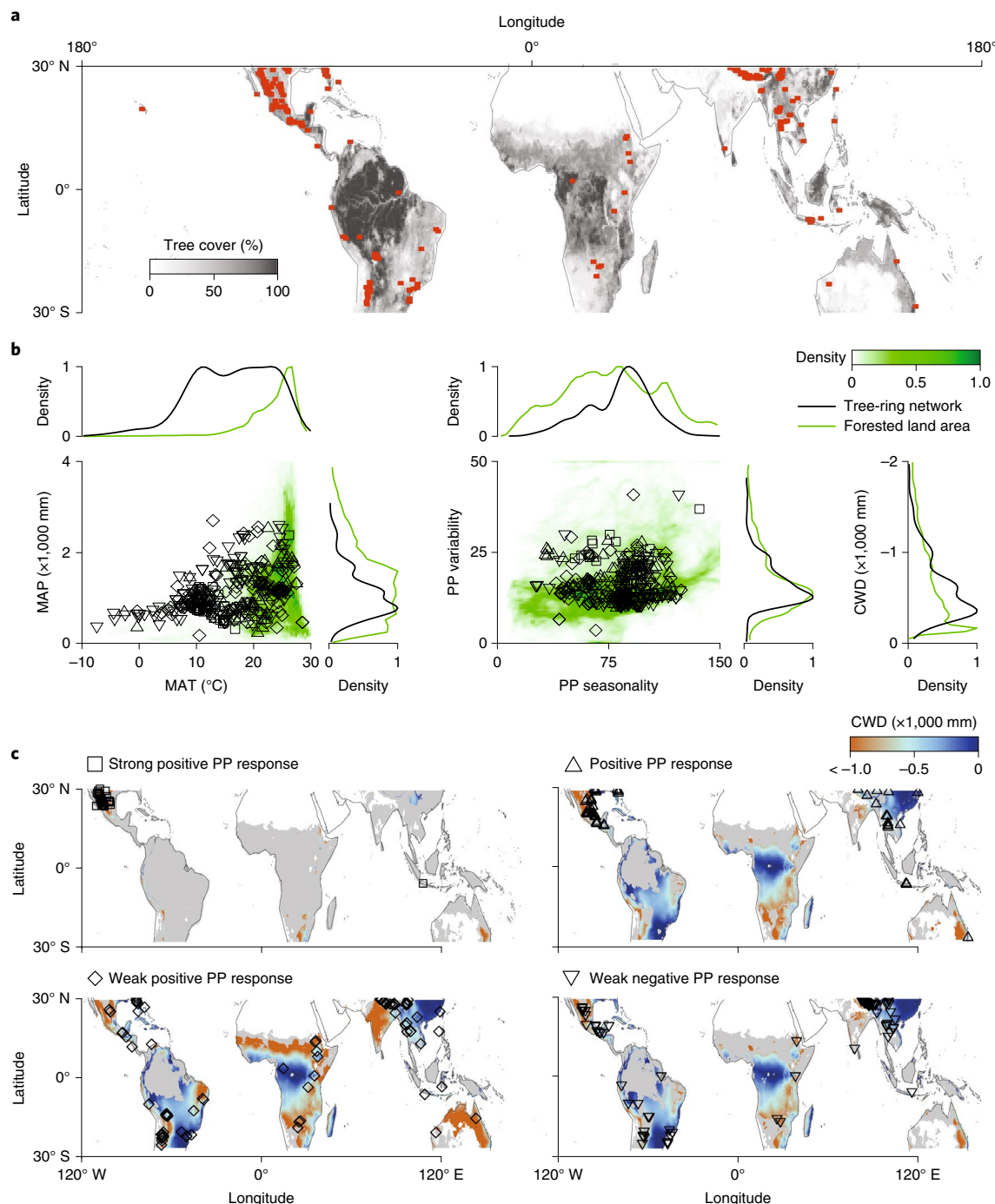
A full list of author and affiliations appears at the end of the paper.

Fig. 1 | Distribution and climatic representativeness of tropical tree-ring network. a, Geographic distribution of tropical tree-ring chronologies ($n = 347$) on a tree-cover map. Tree-cover percentage from open-source data: MODIS (https://lpdaac.usgs.gov/products/mod44bv006/). **b**, Climatic representativeness of the network can be assessed on the basis of distributions of chronologies (black) and tropical land area with woody vegetation (green). Density values are scaled from 0 to 1, with 1 indicating a condition that is most represented in the network (black) or occupies most land area (green). Climatic overrepresentation (underrepresentation) of network occurs when black lines are above (below) green lines. **c**, Geographic distribution of four groups of tropical tree growth responses to climatic variation: strong positive PP response, positive PP response, weak positive PP response and weak negative PP response ($n = 43, 69, 115$ and 120 chronologies, respectively). Maps are coloured by CWD for pixels with woody vegetation falling within group-specific climate envelopes (MAT versus MAP) or are grey for woody vegetation pixels outside envelopes. Groups are representative of 4%, 48%, 67% and 46% of woody vegetated tropical land area, respectively.

pantropical land area with woody vegetation and matches pantropical distributions of precipitation regimes reasonably well (Fig. 1b). The network overrepresents Northern Hemisphere subtropical montane regions, where the presence of coniferous species facilitates dendrochronology, while it underrepresents humid lowland tropical forests, in part because weak climatic seasonality hampers chronology development[26]. We consider these over- and underrepresentations by validation tests and weight-adjusted analyses.

Four robust clusters of climate responses

When SOM clustering the chronologies according to their monthly climate responses, four distinct groups with characteristic climate response modes emerge. Three of the four climate response groups are globally distributed, taxonomically diverse and climatologically representative for 46–67% of global tropical woody vegetation (Fig. 1c). One of the groups (strong positive PP response) is restricted to North America, is taxonomically poor and has a very limited representativeness (4%; Fig. 1c).

Tree growth in three of the four groups responds positively to PP increases and negatively to T_{max} increases, supporting hypothesis 1, whereas these responses are reversed in the fourth group (weak negative PP response; Fig. 2a). Despite differences in response magnitude among the first three groups, the seasonality of the response is similar, with the strongest climate responses occurring in the dry season (Fig. 2a). This larger importance of dry-season climate contrasts with hypothesis 2 and suggests dry-season water availability and demand as first-order drivers of interannual variability in tropical tree growth. The importance of this driver is further supported when ranking the groups from strongly positive PP response to weakly negative PP response. This ranking coincides with a gradient of low to high annual water availability (mean annual precipitation (MAP) and cumulative water deficit (CWD); Fig. 2b) and strongly to weakly negative water balance (Extended Data Table 2), in accordance with hypothesis 3.

In the geographically restricted 'strong positive PP response' group, tree growth reacts strongly and positively to higher PP and lower T_{max} throughout the dry season, with a response peak in the mid-dry season (Fig. 2a). At the semi-arid, high-elevation sites in this group, the mid-dry season occurs in winter, when PP falls primarily as snow and becomes gradually available as moisture during spring when trees resume growth.

Trees in the 'positive PP response' and 'weak positive PP response' groups typically grow at lower elevation, at sites with low to medium water availability (Extended Data Table 2). In both groups, PP response peaks in the late dry season, but the timing and shape of the peaks differ between groups. Finally, the 'weak negative PP response' group occurs at sites with relatively high water availability and is the only group with consistently negative PP and positive T_{max} responses that are somewhat stronger in the wet season compared with the dry season.

The two groups with the strongest positive PP responses differ from each other not only in mean hydroclimatic conditions, but also in the amplitude of interannual PP variation (PP variability) (Fig. 2c). Both annual and dry-season PP variability are stronger for the strong positive PP response group compared with the positive PP response group, indicating that the strongest climate responses can be found at dry sites with high PP variability. By contrast, the two groups with the weakest climate responses show no significant differences in PP variability but differ in their seasonality in precipitation (PP seasonality) (Fig. 2d). Sites with a weakly positive PP response have lower PP seasonality and higher monthly dry-season PP than sites with a weakly negative PP response.

Climate response groups also differed in associations with the El Niño/Southern Oscillation (ENSO) cycle, a major driver of tropical forest productivity[8]. During El Niño years, tree growth in the strong positive PP response group is clearly stimulated, but associations are lacking or weak in the other groups (Extended Data Table 2).

The typical climate responses of these four groups are conserved in cross-validation tests in which a random portion (10%) of the overrepresented colder sites (mean annual temperature (MAT) < 10 °C) was removed (Extended Data Fig. 2a,b). Validation tests in which poorly represented climates (MAP > 2,000 mm) and regions (Africa, Indonesia and Australia) were removed yielded high levels of correct assignments to climate response groups (Extended Data Fig. 2c–e). Region-specific cluster analyses (North America,

High-mountain Asia and South America) show consistent climate responses with the pantropical analysis (Extended Data Fig. 3 and Extended Data Table 3). Thus, the climate response groups identified here are overall robust, unaffected by climatic over-/underrepresentation, and manifest themselves at the regional scale.

Seasonal climate responses vary with hydroclimate

To evaluate the climatic drivers of tropical tree growth at the seasonal level, we constructed multiple regression models for all individual chronologies. In 75% of these 347 regressions, we found at least one significant effect of seasonal PP or T_{max}. The regression coefficients reveal that effects of PP and T_{max} on tree growth are equally large but mostly have opposite signs (PP, positive; T_{max}, negative; Fig. 3a,b), in agreement with hypothesis 1.

Dry-season conditions were a stronger driver than wet-season conditions as indicated by a higher number of significant coefficients (262 dry-season versus 176 wet-season coefficients, dry/wet ratio of coefficients = 1.5), larger absolute coefficient values (Fig. 3c) and higher relative importance values (Fig. 3d) for the dry season. Higher proportions of significant dry-season coefficients were found for all three positive PP effects groups (dry/wet ratio ranging from 1.4 to 3.0). To examine the possible effect of rainfall timing during the late dry season, we ran regression models that included PP and T_{max} during the last two months. While late dry-season climate was often significant in these models, the absolute values of coefficients and their importance values were smaller than those of the full dry season (Extended Data Fig. 4). Together, these results contrast our expectation that tree growth is driven mostly by wet-season climate (hypothesis 2).

Hydroclimatic conditions probably modify these seasonal climate responses. We therefore performed weighted rank correlations between regression coefficients and climatic variables. These correlations show that the predominantly negative effect of dry-season T_{max} on tree growth is stronger at sites that are hotter, are more arid or experience a higher PP variability (Fig. 3e–g and Extended Data Fig. 5), supporting hypothesis 3. In addition, we also find that positive dry-season PP effects are stronger at drier sites (Fig. 3e). A notable exception to this general picture is the weaker positive dry-season PP response at the warmest sites (Fig. 3g), which may be caused by stronger evapotranspiration demand, limiting the positive effects of a wetter dry season. The results of the unweighted correlation analyses were similar to the weighted analyses for all tested climate variables except for MAT (Extended Data Table 4). Thus, overall, dry-season climate responses are stronger where water supply is low and evapotranspiration demand is high.

A dominant role for dry-season climate variability

Combined, our regression and cluster analyses show that tropical tree growth variability responds primarily to dry-season climate variation and that this response is amplified in regions that are drier, are hotter, and experience stronger interannual climate variation. The pantropical and multi-decadal scale of our study provides a context to short-term or regional field studies that reported stronger drought-induced growth reduction at more-arid sites[20,27,28] (consistent with our tests of hypothesis 3) or absence of such responses[29,30] (consistent with the weak negative PP response group). The variability of climate responses revealed by our study calls for caution in scaling up results of local or short-term studies[27,29].

Our finding of opposite and additive effects of PP and T_{max} suggests a dominant role of tree water balance (uptake from precipitation minus loss by transpiration) in driving tropical tree growth. This is further supported by increased strength of PP and T_{max} effects at more arid sites. The importance of tree water balance can be understood from the basic biology of xylem cell formation and enlargement[31] and their strong dependence on xylem turgor pressure[32]. Xylem growth is promoted by high soil water availability but
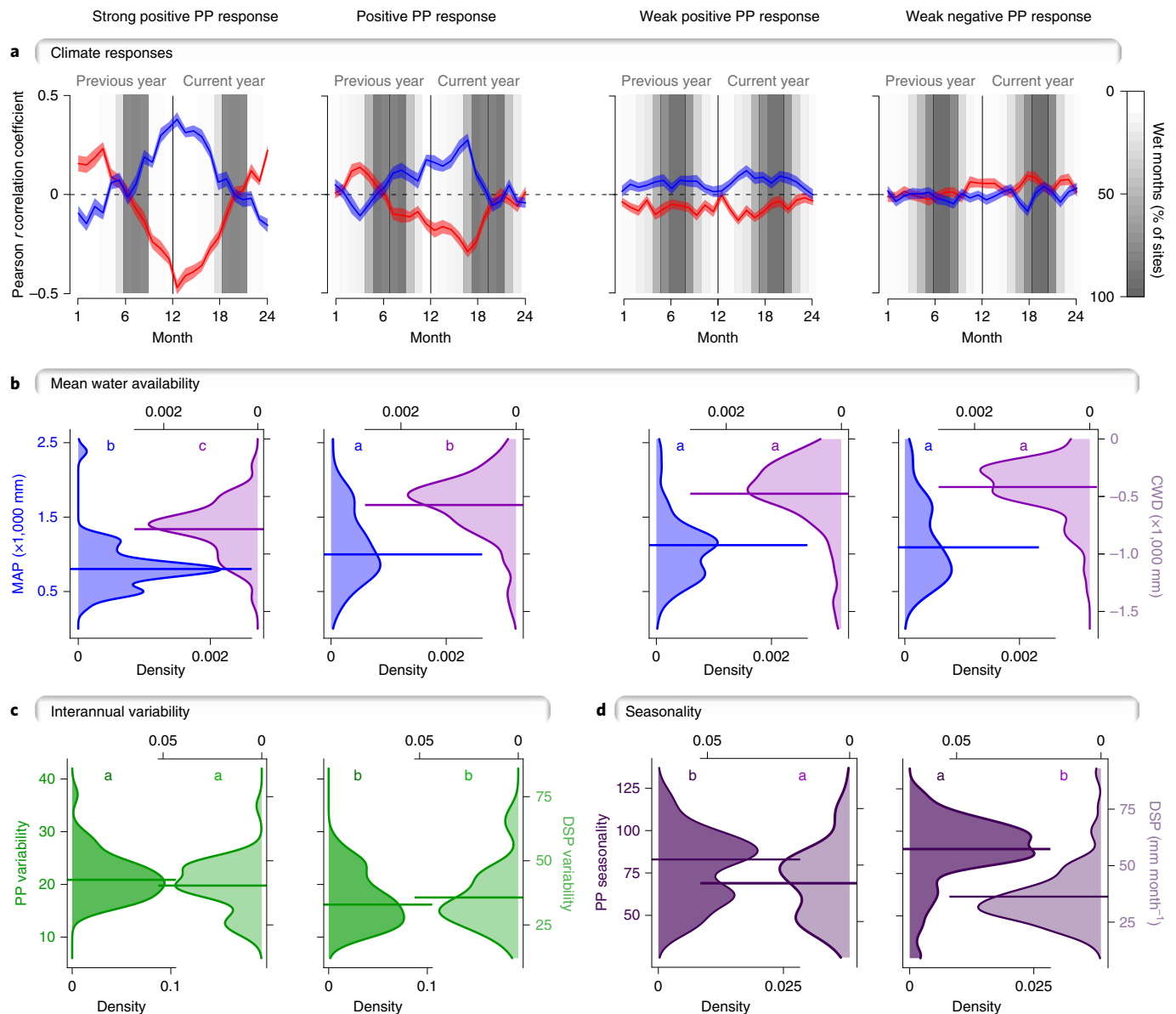
Fig. 2 | Four climate response groups of tropical trees and their hydroclimatic differences. a, Relationships between RWI and interannual variation in monthly T_{max} (red) or PP (blue) of four climate response groups. Shown are Pearson r correlation coefficients (mean and 95% confidence intervals) for a 24 month period that covers the year of ring formation (current) and that before ring formation (previous). Grey shading indicates wet-season timing. **b**, Distribution of mean water availability metrics that distinguish the first two from the last two groups. **c**, Distribution of climate variability metrics that distinguish the strongly positive from the positive PP response group (DSP, dry-season precipitation). **d**, Distribution of climate seasonality that distinguishes the weakly positive from the negative PP response group. Different letters denote significant differences between climate response groups (Wilcoxon rank sum test; $P < 0.05$; Extended Data Table 2). Horizontal lines represent medians.

diminished by T_{max}-induced increase in vapour-pressure deficit and transpiration[27]. Alternative mechanisms explaining the negative temperature effects on growth include T_{max}-induced reduction in photosynthesis and increase in respiration[14], but their contribution is probably small because T_{max} at our sites only rarely exceeds the thermal optimum for photosynthesis (Supplementary Fig. 1) and because negative T_{max} effects occur across a wide range of MAT values (Fig. 3g).

We find that interannual variability in tropical tree growth is explained mostly by climatic variation during the dry season. This result contradicts our second hypothesis that at water-limited sites, wet-season climate drives annual tree growth and hence its interannual variability. How can the climate response of tree growth peak during the dry season when the bulk of productivity of tropical

trees growing in water-limited sites takes place during the wet season[20,27,33–36]? We hypothesize that dry-season climate is more important than wet-season climate because it is more variable (dry-season PP variability = 30.9; wet-season PP variability = 16.5, averaged across network) and because drier months within the dry season lead to direct reduction in tree available water, while the effect of such months during the wet season is probably buffered by soil water reserves[19]. We further hypothesize that climate conditions during the dry season constrain the magnitude of tree growth taking place during the following wet season because climatologically benign dry seasons advance leaf flushing and xylem growth[20,27], thus extending the growing season. Detailed field studies are needed to quantify the physiological and phenological processes responsible
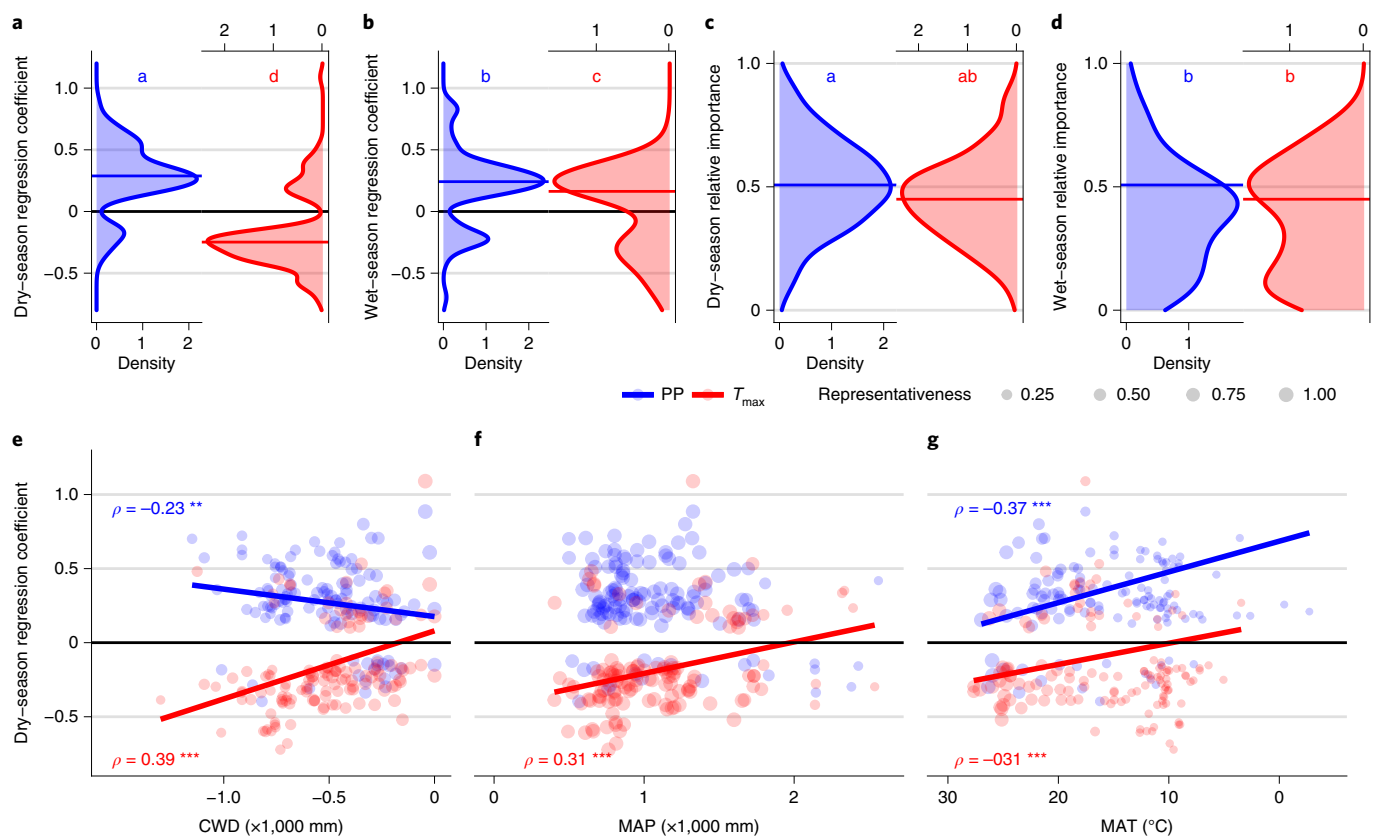
Fig. 3 | Seasonal climate responses of tropical tree growth and their relation to hydroclimate. a,b, Distributions of significant regression coefficients for dry-season (**a**) and wet-season (**b**) T_{max} (red) and PP (blue) in multiple regression models of RWI. Letters denote differences between groups (Wilcoxon rank test, $P < 0.05$, $n = 438$ coefficients; dry season: $n = 262$; wet season: $n = 176$). Horizontal lines represent medians. **c,d,** As panels **a,b** but for dry-season (**c**) and wet-season (**d**) relative importance (models with >1 coefficient, $n = 322$ coefficients). **e–g,** Association of regression coefficients for dry-season PP (blue, $n = 130$) and T_{max} (red, $n = 132$) with site hydroclimate conditions: CWD (**e**), MAP (**f**) and MAT (**g**). Symbol size is proportional to site hydroclimate representativeness (density values, Fig. 1b). Significant associations are indicated (weighted Spearman rank correlation; **$P < 0.01$; ***$P < 0.001$; Extended Data Table 3) and lines are shown for illustration only. All hydroclimatic variables are ordered from arid (left) to humid (right).

for the observed strong dry-season effects and to improve their representation in process-based global vegetation models[37,38].

In addition to mean water availability as a first-order driver, climate responses of tropical tree growth are also modulated by the variability and seasonality in water availability. The effect of interannual variability in precipitation on the climate response of tree growth (Fig. 2c) is consistent with the larger contribution of arid regions to the interannual variation of the global carbon land sink[1,3]. Yet, the modifying role of PP seasonality on climate responses of tropical tree growth is poorly understood. The stronger PP seasonality in the weak negative PP response group (Fig. 2d) may occur if very low moisture availability during the dry season hampers photosynthesis and xylem growth, but also if root access to (deep) soil water during the dry season causes stem growth to be effectively insensitive to dry-season precipitation[39].

The positive T_{max} effects and negative PP effects on tree growth in the weak negative PP response group (Fig. 2a) are probably explained by two distinct mechanisms. At high-elevation sites (>3,000 m above sea level (a.s.l.), 40% of the group), low growing-season temperature may override water availability as the primary constraint of tree growth[40], while at low-elevation sites (<1,500 m a.s.l., 25%), negative PP responses may reflect radiation limitation of photosynthesis[19,20]. Yet, the minimum MAP (2,000 mm) at which radiation limitation is thought to occur[19,20] is not reached by 83% of the low-elevation sites in this group, suggesting that local soil and terrain conditions may alter this generic climatic threshold[19].

Aggravated drought responses under climate change

What shifts in interannual variability of tropical tree growth can be expected under anthropogenic climate change? Global circulation models predict an average 0.5–0.7 °C warming per decade until 2100 for our sites (Extended Data Table 5), probably resulting in stronger water deficits for most of the sites. Drawing from the climatic variation in our network and the shifts in climate responses with MAT, CWD and PP variability, we expect continued climate change and increased PP variability[41] to aggravate negative effects of hotter dry seasons and drier wet seasons on (regional) tree growth (Fig. 3e–g and Extended Data Fig. 5). This stronger sensitivity may elevate tree mortality[42,43], reduce tree longevity[44], and increase the frequency of years that tropical vegetation flips from being a net carbon sink to a net source[8,15,16].

The climate responses of tropical tree growth revealed here may aid the interpretation of interannual variability in the tropical land sink[3,6,10] as they provide field-based and region-specific insights into the climatic drivers of an important component of tropical vegetation productivity.

Online content

Any methods, additional references, Nature Research reporting summaries, source data, extended data, supplementary information, acknowledgements, peer review information; details of author contributions and competing interests; and statements of data and code availability are available at https://doi.org/10.1038/s41561-022-00911-8.

References

1. Ahlström, A. et al. The dominant role of semi-arid ecosystems in the trend and variability of the land CO$_2$ sink. *Science* **348**, 895–899 (2015).
2. Friedlingstein, P. et al. Global carbon budget 2019. *Earth Syst. Sci. Data* **11**, 1783–1838 (2019).
3. Poulter, B. et al. Contribution of semi-arid ecosystems to interannual variability of the global carbon cycle. *Nature* **509**, 600–603 (2014).
4. Fan, L. et al. Satellite-observed pantropical carbon dynamics. *Nat. Plants* https://doi.org/10.1038/s41477-019-0478-9 (2019).
5. Humphrey, V. et al. Sensitivity of atmospheric CO$_2$ growth rate to observed changes in terrestrial water storage. *Nature* **560**, 628–631 (2018).
6. Jung, M. et al. Compensatory water effects link yearly global land CO$_2$ sink changes to temperature. *Nature* **541**, 516–520 (2017).
7. Wang, J., Zeng, N. & Wang, M. Interannual variability of the atmospheric CO$_2$ growth rate: roles of precipitation and temperature. *Biogeosciences* **13**, 2339–2352 (2016).
8. Wigneron, J.-P. et al. Tropical forests did not recover from the strong 2015–2016 El Niño event. *Sci. Adv.* **6**, eaay4603 (2020).
9. Keenan, T. F. & Williams, C. A. The terrestrial carbon sink. *Annu. Rev. Environ. Resour.* **43**, 219–243 (2018).
10. Niu, S. et al. Interannual variability of ecosystem carbon exchange: from observation to prediction. *Glob. Ecol. Biogeogr.* **26**, 1225–1237 (2017).
11. Fatichi, S., Pappas, C., Zscheischler, J. & Leuzinger, S. Modelling carbon sources and sinks in terrestrial vegetation. *N. Phytol.* **221**, 652–668 (2019).
12. Zuidema, P. A., Poulter, B. & Frank, D. C. A wood biology agenda to support global vegetation modelling. *Trends Plant Sci.* **23**, 1006–1015 (2018).
13. Moore, S. et al. Forest biomass, productivity and carbon cycling along a rainfall gradient in West Africa. *Glob. Change Biol.* **24**, e496–e510 (2018).
14. Clark, D. A., Clark, D. B. & Oberbauer, S. F. Field-quantified responses of tropical rainforest aboveground productivity to increasing CO$_2$ and climatic stress, 1997–2009. *J. Geophys. Res. Biogeosci.* **118**, 783–794 (2013).
15. Phillips, O. L. et al. Drought sensitivity of the Amazon rainforest. *Science* **323**, 1344–1347 (2009).
16. Hubau, W. et al. Asynchronous carbon sink saturation in African and Amazonian tropical forests. *Nature* **579**, 80–87 (2020).
17. Pan, Y. et al. A large and persistent carbon sink in the world's forests. *Science* **333**, 988–993 (2011).
18. Anderegg, W. R. L. et al. Climate-driven risks to the climate mitigation potential of forests. *Science* **368**, eaaz7005 (2020).
19. Guan, K. et al. Photosynthetic seasonality of global tropical forests constrained by hydroclimate. *Nat. Geosci.* **8**, 284–289 (2015).
20. Wagner, F. H. et al. Climate seasonality limits leaf carbon assimilation and wood productivity in tropical forests. *Biogeosciences* **13**, 2537–2562 (2016).
21. Zhang, X. et al. Dominant regions and drivers of the variability of the global land carbon sink across timescales. *Glob. Change Biol.* **24**, 3954–3968 (2018).
22. Sullivan, M. J. P. et al. Long-term thermal sensitivity of Earth's tropical forests. *Science* **368**, 869–874 (2020).
23. Hewitson, B. & Crane, R. G. Self-organizing maps: applications to synoptic climatology. *Clim. Res.* **22**, 13–26 (2002).
24. Babst, F. et al. Twentieth century redistribution in climatic drivers of global tree growth. *Sci. Adv.* **5**, eaat4313 (2019).
25. Brienen, R. J., Schöngart, J. & Zuidema, P. A. in *Tropical Tree Physiology* (eds Goldstein, G. & Santiago, L. S.) 439–461 (Springer, 2016).
26. Groenendijk, P., Sass-Klaassen, U., Bongers, F. & Zuidema, P. A. Potential of tree-ring analysis in a wet tropical forest: a case study on 22 commercial tree species in Central Africa. *For. Ecol. Manage.* **323**, 65–78 (2014).
27. Rifai, S. W. et al. ENSO drives interannual variation of forest woody growth across the tropics. *Phil. Trans. R. Soc. B* **373**, 20170410 (2018).
28. López, L., Rodríguez-Catón, M. & Villalba, R. Convergence in growth responses of tropical trees to climate driven by water stress. *Ecography* **42**, 1899–1912 (2019).
29. Doughty, C. E. et al. Drought impact on forest carbon dynamics and fluxes in Amazonia. *Nature* **519**, 78–82 (2015).
30. Clark, D. A., Piper, S. C., Keeling, C. D. & Clark, D. B. Tropical rain forest tree growth and atmospheric carbon dynamics linked to interannual temperature variation during 1984–2000. *Proc. Natl Acad. Sci. USA* **100**, 5852–5857 (2003).
31. Rathgeber, C. B. K., Cuny, H. E. & Fonti, P. Biological basis of tree-ring formation: a crash course. *Front. Plant Sci.* **7**, 734 (2016).
32. Peters, R. L. et al. Turgor—a limiting factor for radial growth in mature conifers along an elevational gradient. *N. Phytol.* **229**, 213–229 (2021).
33. Trouet, V., Mukelabai, M., Verheyden, A. & Beeckman, H. Cambial growth season of brevi-deciduous *Brachystegia spiciformis* trees from south central Africa restricted to less than four months. *PLoS ONE* **7**, e47364 (2012).
34. Mendivelso, H. A., Camarero, J. J., Gutiérrez, E. & Castaño-Naranjo, A. Climatic influences on leaf phenology, xylogenesis and radial stem changes at hourly to monthly scales in two tropical dry forests. *Agric. For. Meteorol.* **216**, 20–36 (2016).
35. Girardin, C. A. J. et al. Seasonal trends of Amazonian rainforest phenology, net primary productivity, and carbon allocation. *Glob. Biogeochem. Cycles* **30**, 700–715 (2016).
36. Krepkowski, J., Bräuning, A., Gebrekirstos, A. & Strobl, S. Cambial growth dynamics and climatic control of different tree life forms in tropical mountain forest in Ethiopia. *Trees* **25**, 59–70 (2011).
37. Restrepo-Coupe, N. et al. Do dynamic global vegetation models capture the seasonality of carbon fluxes in the Amazon basin? A data–model intercomparison. *Glob. Change Biol.* **23**, 191–208 (2017).
38. Barichivich, J. et al. A triple tree-ring constraint for tree growth and physiology in a global land surface model. *Biogeosciences* **18**, 3781–3803 (2021).
39. Nepstad, D. C. et al. The role of deep roots in the hydrological and carbon cycles of Amazonian forests and pastures. *Nature* **372**, 666–669 (1994).
40. Panthi, S., Fan, Z. X., van der Sleen, P. & Zuidema, P. A. Long-term physiological and growth responses of Himalayan fir to environmental change are mediated by mean climate. *Glob. Change Biol.* **26**, 1778–1794 (2020).
41. Morales, M. S. et al. Six hundred years of South American tree rings reveal an increase in severe hydroclimatic events since mid-20th century. *Proc. Natl Acad. Sci. USA* https://doi.org/10.1073/pnas.2002411117 (2020).
42. Brodribb, T. J., Powers, J., Cochard, H. & Choat, B. Hanging by a thread? Forests and drought. *Science* **368**, 261–266 (2020).
43. McDowell, N. G. et al. Pervasive shifts in forest dynamics in a changing world. *Science* **368**, eaaz9463 (2020).
44. Locosselli, G. M. et al. Global tree-ring analysis reveals rapid decrease in tropical tree longevity with temperature. *Proc. Natl Acad. Sci. USA* https://doi.org/10.1073/pnas.2003873117 (2020).

Pieter A. Zuidema [1✉], **Flurin Babst** [2,3], **Peter Groenendijk** [4], **Valerie Trouet** [3], **Abrham Abiyu** [5], **Rodolfo Acuña-Soto** [6], **Eduardo Adenesky-Filho** [7], **Raquel Alfaro-Sánchez** [8], **José Roberto Vieira Aragão** [4], **Gabriel Assis-Pereira** [9,10], **Xue Bai** [11], **Ana Carolina Barbosa** [10], **Giovanna Battipaglia** [12], **Hans Beeckman** [13], **Paulo Cesar Botosso** [14], **Tim Bradley** [15], **Achim Bräuning** [16], **Roel Brienen** [17], **Brendan M. Buckley** [18], **J. Julio Camarero** [19], **Ana Carvalho** [20], **Gregório Ceccantini** [21], **Librado R. Centeno-Erguera** [22], **Julián Cerano-Paredes** [22], **Álvaro Agustín Chávez-Durán** [23], **Bruno Barçante Ladvocat Cintra** [21], **Malcolm K. Cleaveland** [24], **Camille Couralet** [13], **Rosanne D'Arrigo** [18], **Jorge Ignacio del Valle** [25], **Oliver Dünisch** [26], **Brian J. Enquist** [27,28], **Karin Esemann-Quadros** [29,30], **Zewdu Eshetu** [31], **Ze-Xin Fan** [11], **M. Eugenia Ferrero** [32,33], **Esther Fichtler** [34], **Claudia Fontana** [9], **Kainana S. Francisco** [35], **Aster Gebrekirstos** [36], **Emanuel Gloor** [17], **Daniela Granato-Souza** [24], **Kristof Haneca** [37], **Grant Logan Harley** [38], **Ingo Heinrich** [39,40,41], **Gerd Helle** [41], **Janet G. Inga** [33],

Mahmuda Islam[16,42], Yu-mei Jiang [43], Mark Kaib[44], Zakia Hassan Khamisi[3], Marcin Koprowski [45,46], Bart Kruijt [47], Eva Layme[48], Rik Leemans [49], A. Joshua Leffler[50], Claudio Sergio Lisi [51], Neil J. Loader [52], Giuliano Maselli Locosselli[21], Lidio Lopez [32], María I. López-Hernández[53], José Luís Penetra Cerveira Lousada [54], Hooz A. Mendivelso[55], Mulugeta Mokria[16,35], Valdinez Ribeiro Montóia[56], Eddy Moors[57,58], Cristina Nabais[20], Justine Ngoma [59], Francisco de Carvalho Nogueira Júnior[60], Juliano Morales Oliveira [61], Gabriela Morais Olmedo [61], Mariana Alves Pagotto[51], Shankar Panthi [11], Gonzalo Pérez-De-Lis [62], Darwin Pucha-Cofrep [63], Nathsuda Pumijumnong[64], Mizanur Rahman[16,42], Jorge Andres Ramirez [65], Edilson Jimmy Requena-Rojas [33], Adauto de Souza Ribeiro[51], Iain Robertson [52], Fidel Alejandro Roig[32,66], Ernesto Alonso Rubio-Camacho[67], Ute Sass-Klaassen [1], Jochen Schöngart[68], Paul R. Sheppard[3], Franziska Slotta[69], James H. Speer [70], Matthew D. Therrell [71], Benjamin Toirambe[13], Mario Tomazello-Filho[9], Max C. A. Torbenson [72,73], Ramzi Touchan[3], Alejandro Venegas-González[66], Ricardo Villalba [32], Jose Villanueva-Diaz[22], Royd Vinya[74], Mart Vlam[75], Tommy Wils [76] and Zhe-Kun Zhou [11]

[1]Forest Ecology and Forest Management Group, Wageningen University, Wageningen, the Netherlands. [2]School of Natural Resources and the Environment, University of Arizona, Tucson, AZ, USA. [3]Laboratory of Tree-Ring Research, University of Arizona, Tucson, AZ, USA. [4]Department of Plant Biology, Institute of Biology, University of Campinas (UNICAMP), Campinas, Brazil. [5]World Agroforestry Centre (ICRAF), Addis Ababa, Ethiopia. [6]Department of Microbiology and Parasitology, Universidad Nacional Autónoma de México, Mexico City, Mexico. [7]Laboratory of Protection and Forest Management, Department of Forest Engineering, Universidade Regional de Blumenau, Santa Catarina, Brazil. [8]Department of Biology, Wilfrid Laurier University, Waterloo, Ontario, Canada. [9]Department of Forest Sciences, Luiz de Queiroz College of Agriculture, University of Sao Paulo, Piracicaba, Brazil. [10]Tree-Ring Laboratory, Forest Science Department, Federal University of Lavras, Lavras, Brazil. [11]CAS Key Laboratory of Tropical Forest Ecology, Xishuangbanna Tropical Botanical Garden, Chinese Academy of Sciences, Mengla, China. [12]Department of Environmental, Biological and Pharmaceutical Sciences and Technologies, University of Campania "L. Vanvitelli", Caserta, Italy. [13]Service of Wood Biology, Royal Museum for Central Africa, Tervuren, Belgium. [14]Brazilian Agricultural Research Corporation (Embrapa), Embrapa Forestry, Colombo, Brazil. [15]U.S. Department of Agriculture, Forest Service, NWCG Member Agency, Washington, DC, USA. [16]Institute of Geography, Friedrich-Alexander-University Erlangen-Nuremberg, Erlangen, Germany. [17]School of Geography, University of Leeds, Leeds, UK. [18]Lamont-Doherty Earth Observatory, Columbia University, Palisades, NY, USA. [19]Instituto Pirenaico de Ecología (IPE-CSIC), Zaragoza, Spain. [20]Centre for Functional Ecology, Department of Life Sciences, Faculty of Sciences and Technology, University of Coimbra, Coimbra, Portugal. [21]Department of Botany, Institute of Biosciences, University of São Paulo, São Paulo, Brazil. [22]Instituto Nacional de Investigaciones Forestales, Agrícolas y Pecuarias (INIFAP), Centro Nacional de Investigación Disciplinaría en Relación Agua-Suelo-Planta-Atmósfera (CENID-RASPA), Gómez Palacio, México. [23]Instituto Nacional de Investigaciones Forestales, Agrícolas y Pecuarias (INIFAP), Campo Experimental Centro - Altos de Jalisco, Tepatitlán de Morelos, México. [24]Department of Geosciences, University of Arkansas, Fayetteville, AR, USA. [25]Department of Forest Sciences, Universidad Nacional de Colombia - Sede Medellín, Medellín, Colombia. [26]Master School for Carpentry and Cabinetmaking, Ebern, Germany. [27]Department of Ecology and Evolutionary Biology, University of Arizona, Tucson, AZ, USA. [28]Santa Fe Institute, Santa Fe, NM, USA. [29]Department of Biological Sciences, University of Joinville Region - UNIVILLE, Joinville, Brazil. [30]Postgraduate Program in Forestry, Regional University of Blumenau - FURB, Blumenau, Brazil. [31]College of Life Science, Climate Science Center and Department of Earth Science, Addis Ababa University, Addis Ababa, Ethiopia. [32]Departamento de Dendrocronología e Historia Ambiental, IANIGLA, CCT-CONICET-Mendoza, Mendoza, Argentina. [33]Laboratorio de Dendrocronología, Universidad Continental, Huancayo, Perú. [34]Department of Crop Sciences, Tropical Plant Production and Agricultural Systems Modelling, Göttingen University, Göttingen, Germany. [35]Institute of Pacific Islands Forestry, USDA Forest Service Pacific Southwest Research Station, Hilo, HI, USA. [36]World Agroforestry Centre (ICRAF), Nairobi, Kenya. [37]Flanders Heritage Agency, Brussels, Belgium. [38]Department of Geography and Geological Sciences, University of Idaho, Moscow, ID, USA. [39]German Archaeological Institute DAI, Berlin, Germany. [40]Geography Department, Humboldt University Berlin, Berlin, Germany. [41]GFZ German Research Centre for Geosciences, Potsdam, Germany. [42]Department of Forestry and Environmental Science, Shahjalal University of Science and Technology, Sylhet, Bangladesh. [43]Faculty of Forestry and Wood Sciences, Czech University of Life Sciences Prague, Prague, Czech Republic. [44]US Fish and Wildlife Service, Albuquerque, NM, USA. [45]Department of Ecology and Biogeography, Faculty of Biological and Veterinary Sciences, Nicolaus Copernicus University, Toruń, Poland. [46]Centre for Climate Change Research, Nicolaus Copernicus University, Toruń, Poland. [47]Water Systems and Global Change Group, Wageningen University and Research, Wageningen, the Netherlands. [48]Instituto Nacional de Innovación Agraria, Programa Nacional de Investigación Forestal, Huancayo, Perú. [49]Environmental Systems Analysis Group, Wageningen University and Research, Wageningen, the Netherlands. [50]Department of Natural Resource Management, South Dakota State University, Brookings, USA, SD. [51]Laboratory of Plant Anatomy and Dendrochronology, Department of Biology, Universidade Federal de Sergipe, Sergipe, Brazil. [52] Department of Geography, Swansea University, Swansea, UK. [53]Departamento Forestal, Universidad Autónoma Agraria Antonio Narro, Saltillo, Mexico. [54]CITAB - Department of Forestry Sciences and Landscape (CIFAP), University of Trás-os-Montes and Alto Douro, Vila Real, Portugal. [55]Escuela de Ciencias Biológicas, Universidad Pedagógica y Tecnológica de Colombia (UPTC), Tunja, Colombia. [56]Brazilian Agricultural Research Corporation (Embrapa), Embrapa Amazônia Ocidental, Manaus, Brazil. [57]IHE Delft, Delft, the Netherlands. [58]VU University Amsterdam, Amsterdam, the Netherlands. [59]Department of Biomaterials Science and Technology, School of Natural Resources, The Copperbelt University, Kitwe, Zambia. [60]Laboratory of Ecology and Dendrology of the Federal Institute of Sergipe, São Cristovão, Brazil. [61]Laboratory of Plant Ecology, Universidade do Vale do Rio dos Sinos (UNISINOS), São Leopoldo, Brazil. [62]BIOAPLIC, Departamento de Botánica, Universidade de Santiago de Compostela, EPSE, Lugo, Spain. [63]Laboratorio de Dendrocronología, Carrera de Ingeniería Forestal, Universidad Nacional de Loja, Loja, Ecuador. [64]Faculty of Environment and Resource studies, Mahidol University, Nakhon Pathom, Thailand. [65]Facultad de Ciencias Agrarias, Universidad del Cauca, Popayán, Colombia. [66]Hémera Centro de Observación de la Tierra, Escuela de Ingeniería Forestal, Facultad de Ciencias, Universidad

Mayor, Santiago, Chile. [67]Instituto Nacional de Investigaciones Forestales, Agrícolas y Pecuarias (INIFAP), Centro de Investigación Regional Pacífico Centro - Campo Experimental, Centro Altos de Jalisco, México. [68]National Institute for Amazon Research, Petrópolis, Manaus, Brazil. [69]Department of Earth Sciences, Freie Universität Berlin, Berlin, Germany. [70]Department of Earth and Environmental Systems, Indiana State University, Terre Haute, IN, USA. [71]Department of Geography, University of Alabama, Tuscaloosa, AL, USA. [72]Department of Civil, Environmental and Geodetic Engineering, The Ohio State University, Columbus, OH, USA. [73]Department of Geography, Johannes Gutenberg University, Mainz, Germany. [74]Department of Plant and Environmental Sciences, School of Natural Resources, The Copperbelt University, Kitwe, Zambia. [75]Forest and Nature Management, Van Hall Larenstein University of Applied Sciences, Velp, the Netherlands. [76]School of Teacher Training for Secondary Education Tilburg, Fontys University of Applied Sciences, Tilburg, the Netherlands. ✉e-mail: Pieter.Zuidema@wur.nl

Methods

Tree-ring network. We established our tropical tree-ring network (https://tropicaltreeringnetwork.org/) by compiling published ring-width chronologies from naturally regenerating tree populations in tropical and subtropical vegetation (30° N to 30° S; excluding mangroves and flooded forests). For this purpose, we compiled raw ring-width data from the ITRDB (https://www.ncdc.noaa.gov/data-access/paleoclimatology-data/datasets/tree-ring; 241 chronologies). To increase representation of wetter tropical regions[45,25], we complemented this dataset with 174 chronologies derived from published tree-ring studies (mainly low-latitude sites; Extended Data Fig. 1).

Chronology selection. From the initial 415 chronologies, we selected those with a minimum length of 50 years, based on at least 5 trees and ending after 1975. The 1975 cut-off date is a compromise between the low quality of early-twentieth-century gridded climate data and the sharp recent decline in tree-ring data[46]. In addition, we selected chronologies with a mean inter-series correlation (Rbar) greater than 0.3 over the 50 yr period. Low or non-significant Rbar values may indicate poor dating quality, a lack of common environmental drivers of growth[26,47] or both and are expected in wetter climates. By introducing an Rbar threshold, which removed 9% of chronologies, we sought a compromise between ensuring chronology quality and being overly selective towards highly climate-sensitive chronologies.

Our selection procedure removed 68 chronologies (6 ITRDB and 62 contributed). The resulting network includes 347 chronologies (235 from ITRDB, 112 from contributors) and is based on 7,751 trees and 14,032 series from 99 species (56 genera, 24 families; metadata in Supplementary Data). Species are represented by 1–49 chronologies (average = 3.4) and by an average of 21.5 trees.

The selected chronologies were originally developed for various purposes, including climate reconstructions, ecological studies and timber yield evaluations. Dendroclimatic reconstructions are usually conducted in marginal habitats in arid and high montane regions[48], which may introduce a 'macro-site selection bias' in tree-ring networks. Such bias can be strong (for instance, in the arid Southwest of the United States[49]) but was not found to exist when ITRDB chronologies were compared with independent reference networks (fig. S7 in ref. [24] and fig. [3] in ref. [50]). We accommodated possible macro-site selection bias in our network by calculating and accounting for the climatic representativeness of sites (Network representativeness)[49].

Chronology building and quality control. To ascertain homogeneous data treatment across trees and sites, we applied the same detrending method to all individual raw ring-width series to develop tree-ring chronologies rather than using the published chronologies. We tested various detrending methods that account for ontogeny, remove low-frequency variation and retain the high-frequency (annual) variation we study here. We selected a flexible spline detrending with a 50% frequency cut-off at 30 years to emphasize the interannual variation in ring width. We developed mean chronologies of RWI from the detrended series using a bi-weight robust mean, and the most recent 50 years of each chronology were selected for analysis. We ensured that dating of all tree-ring series from the Southern Hemisphere followed the Schulman convention[51], such that the calendar year assigned to the ring is that during which ring formation started. An exception was made for the Southern Hemisphere chronologies in the Brazilian Caatinga biome, where the growth season occurs between March and July[52] and thus coincides with the Northern Hemisphere's growth season, making the Shulman shift redundant. Detrending and chronology building were conducted in R (ref. [53]) using the dplR package[54].

Woody vegetation and elevation data. To relate climate responses to tree cover, we obtained MODIS- (moderate-resolution imaging spectroradiometer) derived tree-cover percentages for all sites ('Percent_Tree_Cover', MOD44B version 6; https://lpdaac.usgs.gov/products/mod44bv006/). We also used this data product to mask out areas with <10% tree cover of tropical land area.

Climate data. We used three types of gridded climate data. We used Worldclim version 2 (worldclim.org)[55] to obtain 30 yr (1970–2000) mean annual and monthly climate conditions at 1 km spatial resolution. This yielded data on mean monthly PP, total dry-season precipitation (DSP, in millimetres), total wet-season precipitation (WSP, in millimetres), MAP (in millimetres), MAT (in °C) and PP seasonality (unitless; this is the coefficient of variation of monthly PP (ref. [55])). In addition, we calculated the monthly climatic water balance (CWB) as the difference between monthly precipitation and potential evapotranspiration (PP-PET). PET was estimated from monthly Worldclim climate parameters using the Penman–Monteith equation implemented in the SPEI package in R (ref. [56]). From these data, we derived, per site, annual CWD (in millimetres; always negative) as the sum of all negative monthly CWDs, annual CWB (in millimetres) as the sum of all monthly CWBs, and maximum monthly water deficit (MMWD, in millimetres) as the lowest (most negative) value of monthly CWBs. This set of variables was used to characterize climatic site conditions for all chronologies.

We further used Worldclim to obtain CMIP6 downscaled future climate projections for periods 2041–2060 and 2061–2080 (compared with 1970–2000)

for all sites. We used two shared socioeconomic pathways (370 and 585) and nine global circulation models, of which we calculated an ensemble (arithmetic) mean across sites and models.

Third, we used Climate Research Unit TS4.02 (ref. [57]) climate data to conduct climate–growth analyses based on monthly time series at a coarser spatial resolution (0.5°) for the most recent 50 years of each chronology in our network. Such broader-resolution gridded data do not optimally capture elevational climate gradients, but they provide the homogeneity and long time series needed to establish climate–growth relations in our cluster and regression analyses. All climate–growth analyses were conducted for daily T_{max} (averaged per month or season) and PP (sum per month or season). We chose to use T_{max} as it is related to atmospheric drought (vapour-pressure deficit) and thus to the tree water balance, which we hypothesized to be an important driver of tropical tree growth. Climate Research Unit data were also used to obtain a metric of PP variability for all sites and for all tropical land with woody vegetation. PP variability was calculated as the coefficient of variation of the PP time series over the 50 years covered by the tree-ring chronologies.

Season definitions. The multiple regression models (Multiple regression analysis) were constructed for seasonal (wet and dry season) PP and T_{max}. We tested various season definitions based on PP and CWB: seasons based on a monthly PP cut-off of 50 and 100 mm (ref. [25]) and based on CWB calculated using the Thornthwaite and the Penman–Monteith equations. Seasonal boundaries were very similar for 100 mm PP and CWB (Penman–Monteith) definitions, and we thus selected the 100 mm cut-off definition for its simplicity and because variables such as wind speed required for CWB are associated with large uncertainties in gridded data. The dry season was thus defined as all months with less than 100 mm precipitation preceding the wet season of the year of ring formation.

Frequency of hot months. To estimate to what extent T_{max} may limit tree growth through decreased photosynthesis, we calculated per site the percentage of months during which T_{max} exceeded 30 °C, when leaves in sun-exposed crowns can reach temperatures >32 °C and reduce photosynthesis[58,59]. If a large proportion of sites frequently experience such high T_{max} values, this suggests an important role of temperature-driven photosynthetic limitation in tropical tree growth. If that proportion is small, it suggests that negative effects of T_{max} on tropical tree growth are resulting mainly from increased transpiration.

Network representativeness. We evaluated the climatic representativeness of our network in two ways. First, we used Worldclim average climate data for all sites to define the climate space of our network and the four climate response groups (Cluster analysis) using a convex hull that encompasses 99% of the network's MAP and MAT range (to minimize edge effects). Grid cells with MAP–MAT combinations outside this contour shape are not represented by our network and masked from CWD maps (Fig. 1c). Climatic representativeness was estimated by calculating the percentage of pixels of tropical land area with >10% woody vegetation (49,870,418 km²) within the convex hull.

Second, we quantified the representativeness of our network for tropical vegetation by comparing the probability density distributions of geographic and climatic variables (CWD, MAP, PP seasonality, PP variability, MAT) across our sites with those of all tropical land area that supports woody vegetation (>10% tree cover). We scaled both sets of distributions (sites and land area) by dividing them by their maximum values. Thus, a scaled value of 0 implies that the corresponding climatic condition is not represented by sites or tropical land area; a value of 1 implies that the climatic condition has the highest representation of sites or land area. When the scaled distributions of the network (black lines in Fig. 1b) and tropical land area (green lines) are similar, overall representativeness is good (for example, MAT, PP variability; Fig. 1b); if they are dissimilar, overall representativeness is limited (for example, MAT). For each climatic variable, a higher value of the network compared with the tropical land area indicates overrepresentation in the network, while the reverse indicates underrepresentation. We use the scaled distributions of land area for weighted correlations in our analysis of shifts in climate responses along climatic gradients (Climate responses versus climatic conditions). In two-dimensional space (Fig. 1b), distributions were calculated using bivariate kernel density estimation (GenKern package[60]).

Cluster analysis. Seasonal climate–growth analyses can miss subtle, idiosyncratic responses of tree species to climatic conditions during specific months or with a lag period. To accommodate such responses, we conducted monthly climate–growth analyses (simple Pearson correlations) for a 24 month period (full year of ring formation, plus full previous year) and used these as a basis for clustering. For Northern Hemisphere sites, the 24 month period starts in January of the year before ring formation and ends in December of the year of ring formation. For Southern Hemisphere sites, this period is lagged by six months (running from 1 July to June). We identified distinct groups of sites with a coherent climate response using SOMs[23]. SOMs are an artificial neural network-based method of dimension reduction that assigns observations (chronologies) to a set of clusters (or 'nodes') on the basis of Euclidean distance. In an iterative process, the optimal node assignment is determined in an unsupervised manner to best represent the

dataset's variance. Nodes are then arranged in a grid of definable size and shape; closer nodes in this grid are more similar, distant nodes are dissimilar. This feature greatly facilitates the visualization and interpretation of nodes, as has previously been shown in regional- and continental-scale tree-ring studies[61,62].

We calculated SOMs on the basis of the monthly climate correlations. The algorithm was presented with 24 T_{max} correlations and 24 PP correlations per site, but no other information (for example, site location or climate). We tested square SOM grids of increasing size (2×2, 3×3 and so on) to visualize increasingly nuanced differences in climate response between the nodes. Then, we calculated bootstrapped means (1,000 replicates) and 95% confidence intervals of the climate correlations from all sites (Fig. 2a) or of geographic sub-regions (Extended Data Fig. 4) that were assigned to a given node. We present the results based on the 2×2 SOM grid (four climate response groups). Further subdivision did not result in additional modes of climate response but merely in minimally differing variants of the four main groups. While SOM clustering uses all subtleties of site-specific responses of RWI to monthly climate conditions, the resulting climate responses are an average across all sites within a cluster and may therefore differ from site-specific correlation patterns. Despite this possible discrepancy, SOM clustering optimizes the representation of idiosyncratic and subtle climate responses of tree growth.

One challenge associated with SOMs is that their initiation is random, which leads to minor differences in site assignments. To overcome this challenge, we stabilized the grouping iteratively in 10,000 consecutive SOM runs. In each run, the codebook vectors (representing the mean climate correlations within a node) were reassigned to an existing node with the most-similar codebook vector based on all previous runs. This codebook vector was then updated with the new vector. For the final site assignment, we considered only the last 1,000 runs, when the codebook vectors did not change much anymore. The percentage of those runs when a site was assigned to a given node (for example, site X was assigned to Node1 in 900 out of 1,000 runs = 90%) was used as a quality measure for the clustering. Percentage assignments were high: $93 \pm 10\%$ (mean ± 1 s.d.) across the entire network and ranging from 85% to 97% (means) per cluster. These analyses were performed using the kohonen[63] and boot[64] packages in R.

To compare climate and geographic characteristics of the four climate response groups, we performed non-parametric analyses of variance (Kruskal–Wallis rank sum test) followed by a Wilcoxon rank sum post hoc test.

Validation tests of cluster analysis results. To evaluate the robustness of our cluster results regarding the over- and underrepresentation of climatic conditions and regions, we performed four sets of validation tests. In these 'leave-several-out cross-validation' tests, we removed a number of chronologies from the network: (1) a random subset to test overall robustness (10%, repeated 10 times); (2) all 'cold' sites (<10 °C MAT) to test whether clustering is strongly driven by high-elevation sites that are overrepresented in our network; (3) all 'wet' sites (>2,000 mm MAP) and (4) all sites in underrepresented regions (Africa, Indonesia and Australia), with the goal to verify whether low representation of climates or regions affects the assignment of chronologies to climate response groups. After removing the sites, we reconducted the cluster analyses (as described in Cluster analysis) for the remaining chronologies. Each of the removed sites was then 'assigned' to one of the four clusters by calculating monthly climate-growth correlations with all four clusters and assigning it to the cluster with the most-similar climate correlation patterns (smallest average difference in monthly correlations). We then calculated the percentage of correct assignments (to the same cluster as in the original clustering approach) and compared monthly climate correlation patterns (Extended Data Fig. 2) with those of the main analysis (Fig. 2a). Clustering results were considered robust if correlation patterns remained similar and the percentage of correct assignments was high.

Evaluating sensitivity of climate responses to quality of gridded climate data. To evaluate possible biases introduced by spatially varying quality of gridded climate data, we performed two analyses using distance of sites to the nearest meteorological station (from https://climexp.knmi.nl) as a proxy for the quality of gridded data. For the majority of sites, proximal meteorological stations exist: distances between sites and stations ranged from 0 to 243 km (median: 63 km) and were >100 km for 93 sites (27%). For analysis 1, we evaluated associations between the seasonal climate response and the distance to the nearest station. Because climate responses are driven by mean climate, we performed this analysis within two-way climate bins of MAP (300 mm wide) and MAT (3 °C wide). Within each climate bin that contained at least ten sites, we associated the climate response (the P value of the Pearson correlation of RWI with PP or T_{max} during dry or wet season) with distance to the nearest meteorological station using Spearman rank correlation. Positive Spearman correlations indicate that correlation strength is higher when meteorological station density is higher (Extended Data Table 1a). For analysis 2, to verify the extent to which climate responses in our four clusters are modulated by the density of meteorological stations, we used t tests to find differences in correlation coefficients of RWI and monthly climate (PP and T_{max}) between sites located <100 km and >100 km from meteorological stations. We conducted tests for the two climate response groups with a sufficiently large number ($n > 10$) of sites at >100 km from meteorological stations and for the 24 month period used in our cluster analysis (Extended Data Table 1b).

Multiple regression analysis. For each chronology, we ran a multiple regression model to evaluate additive effects on RWI of interannual variability in seasonal T_{max} and PP, which typically co-vary. This approach allows for controlling for one variable while testing the effect of another and yields additive effects in case multiple variables are included. To prevent model overfitting, we limited the number of explanatory variables (summed PP and average T_{max}) and conducted seasonal (rather than monthly) analyses. The maximum number of climate variables in the models is thus 4 for a fixed chronology length of 50 years. We used the leaps algorithm for model selection, an all-subset model comparison[65] that is more robust than stepwise methods. We scaled climate variables; their effects on tree growth are therefore directly comparable and unaffected by season length. We checked for collinearity between PP and T_{max} and found significant, mostly negative, associations in 73% (wet) and 59% (dry) of cases. We therefore checked variance inflation factors in all models and found these to be lower than 2.2. To compare the relative strengths of PP and T_{max} effects on tree growth, we calculated relative importance values of significant climate variables. These are reported only for models with >1 significant coefficient.

To examine whether dry-season effects were mostly driven by PP over the entire dry season or in the transitional months from dry to wet season (the 'Late dry season'), we also ran all regression models with two additional climate variables, summed PP and average T_{max}, over the two last months of the dry season and then compared number of significant coefficients, absolute coefficient values and relative importance values of full versus late dry season (Extended Data Fig. 4). Analyses were conducted in R using packages leaps[66], bestglm[67] and relaimpo[68].

Climate responses versus climatic conditions. To evaluate whether seasonal climate responses of tree growth are associated with site hydroclimate, we correlated significant regression coefficients with site climatic conditions: CWD, MAP, MAT, PP variability and PP seasonality. We performed ordinary as well as weighted Spearman rank correlations to account for climate representativeness of sites. We weighted data points by the relative density of tropical land area with woody vegetation for each climate variable (the green lines in Fig. 1b; Network representativeness). Thus, low-MAT sites (overrepresented in network) received a lower weight than high-MAT sites. Analyses were conducted in R using package expss[69].

Reporting Summary. Further information on research design is available in the Nature Research Reporting Summary linked to this paper.

Data availability
The 50-year mean RWI time series of all 347 chronologies used in this study and all relevant metadata of these chronologies are included in Supplementary Data. Raw tree-ring-width data of 98 out of the 112 contributed chronologies used in the analyses have been uploaded to the ITRDB (https://www.ncdc.noaa.gov/data-access/paleoclimatology-data/datasets/tree-ring).

Code availability
R-code used for chronology construction and statistical analyses will be made available upon request from the corresponding author.

References
45. Zhao, S. et al. The International Tree-Ring Data Bank (ITRDB) revisited: data availability and global ecological representativity. *J. Biogeogr.* **46**, 355–368 (2019).
46. Babst, F., Poulter, B., Bodesheim, P., Mahecha, M. D. & Frank, D. C. Improved tree-ring archives will support Earth-system science. *Nat. Ecol. Evol.* **1**, 0008 (2017).
47. Fichtler, E., Clark, D. A. & Worbes, M. Age and long-term growth of trees in an old-growth tropical rain forest, based on analyses of tree rings and ^{14}C. *Biotropica* **35**, 306–317 (2003).
48. Fritts, H. *Tree Rings and Climate* (Elsevier, 2012).
49. Klesse, S. et al. Sampling bias overestimates climate change impacts on forest growth in the southwestern United States. *Nat. Commun.* **9**, 5336 (2018).
50. Klesse, S. et al. A combined tree ring and vegetation model assessment of European forest growth sensitivity to interannual climate variability. *Glob. Biogeochem. Cycles* **32**, 1226–1240 (2018).
51. Schulman, E. *Dendroclimatic Changes in Semiarid America* (Univ. Arizona Press, 1956).
52. Aragão, J. R. V., Groenendijk, P. & Lisi, C. S. Dendrochronological potential of four neotropical dry-forest tree species: climate–growth correlations in northeast Brazil. *Dendrochronologia* **53**, 5–16 (2019).
53. R Core Team *R: A Language and Environment for Statistical Computing* (R Foundation for Statistical Computing, 2019).
54. Bunn, A. G. A dendrochronology program library in R (dplR). *Dendrochronologia* **26**, 115–124 (2008).
55. Fick, S. E. & Hijmans, R. J. WorldClim 2: new 1-km spatial resolution climate surfaces for global land areas. *Int. J. Climatol.* **37**, 4302–4315 (2017).
56. Vicente-Serrano, S. M., Beguería, S. & López-Moreno, J. I. A multiscalar drought index sensitive to global warming: the Standardized Precipitation Evapotranspiration Index. *J. Clim.* **23**, 1696–1718 (2010).

57. Harris, I., Jones, P. D., Osborn, T. J. & Lister, D. H. Updated high-resolution grids of monthly climatic observations—the CRU TS3.10 Dataset. *Int. J. Climatol.* **34**, 623–642 (2014).
58. Pau, S., Detto, M., Kim, Y. & Still, C. J. Tropical forest temperature thresholds for gross primary productivity. *Ecosphere* **9**, e02311 (2018).
59. Mau, A., Reed, S., Wood, T. & Cavaleri, M. Temperate and tropical forest canopies are already functioning beyond their thermal thresholds for photosynthesis. *Forests* **9**, 47 (2018).
60. Lucy, D., Aykroyd, R. G. & Pollard, A. M. Nonparametric calibration for age estimation. *J. R. Stat. Soc. C* **51**, 183–196 (2002).
61. Babst, F. et al. Site- and species-specific responses of forest growth to climate across the European continent. *Glob. Ecol. Biogeogr.* **22**, 706–717 (2013).
62. Martin-Benito, D. & Pederson, N. Convergence in drought stress, but a divergence of climatic drivers across a latitudinal gradient in a temperate broadleaf forest. *J. Biogeogr.* **42**, 925–937 (2015).
63. Wehrens, R. & Buydens, L. M. Self- and super-organizing maps in R: the kohonen package. *J. Stat. Softw.* https://doi.org/10.18637/jss.v021.i05 (2007).
64. Canty, A. & Ripley, B. D. boot: Bootstrap R (S-Plus) Functions. R package v.1.3-26 (2021).
65. Furnival, G. M. & Wilson, R. W. Regressions by leaps and bounds. *Technometrics* **16**, 499–511 (1974).
66. Lumley, T. leaps: Regression Subset Selection. R package v.3.1 (2019).
67. McLeod, A. I., Xu, C. & Lai, Y. bestglm: Best Subset GLM and Regression Utilities. R package v.0.37.3 (2020).
68. Groemping, U. Relative importance for linear regression in R: the package relaimpo. *J. Stat. Softw.* https://doi.org/10.18637/jss.v017.i01 (2006).
69. Demin, G. & Jeworutzki, S. expss: Tables, Labels and Some Useful Functions from Spreadsheets and 'SPSS' Statistics. R package v.0.10.7 (2020).
70. Whittaker, R. H. *Primary Productivity of the Biosphere* Vol. 14 (Springer-Verlag, 1975).
71. Beck, H. E. et al. Present and future Köppen-Geiger climate classification maps at 1-km resolution. *Sci. Data* **5**, 180214 (2018).

Author contributions

P.A.Z., P.G. and V.T. initiated the tropical tree-ring network; P.A.Z., F.B., P.G. and V.T. designed the study; all co-authors except F.B. contributed tree-ring data; F.B. and P.G. analysed the data, with important contributions from P.A.Z.; P.A.Z. and V.T. wrote the manuscript, with important contributions from F.B. and P.G. All co-authors read and approved the manuscript.

Competing interests

The authors declare no competing interests.

Additional information

Extended data is available for this paper at https://doi.org/10.1038/s41561-022-00911-8.

Supplementary information The online version contains supplementary material available at https://doi.org/10.1038/s41561-022-00911-8.

Correspondence and requests for materials should be addressed to Pieter A. Zuidema.

Peer review information *Nature Geoscience* thanks Amy Hessl and the other, anonymous, reviewer(s) for their contribution to the peer review of this work. Primary Handling Editor: Tom Richardson, in collaboration with the *Nature Geoscience* team.

Reprints and permissions information is available at www.nature.com/reprints.
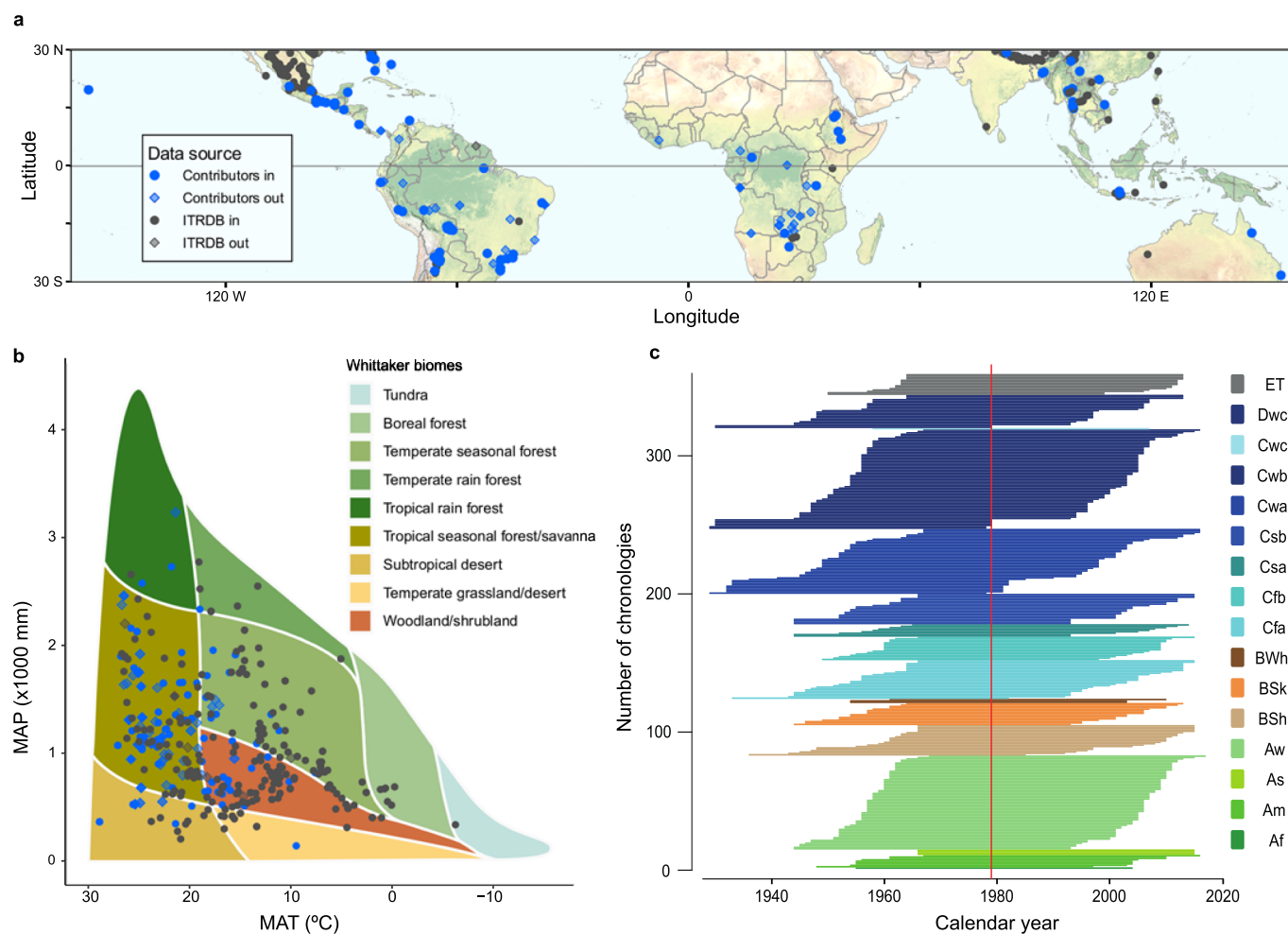
Extended Data Fig. 1 | Distribution and characteristics of the 415 chronologies in the network. a, Spatial distribution of tree-ring chronologies from two sources (ITRDB and contributors) selected to be included in this study ("in", $n = 347$) or not ("out", $n = 68$). **b,** Chronology distribution in climate space and across tropical biomes following Whittaker biome classification[70]. **c,** Distribution of the most recent 50 years of selected chronologies in time and across Koeppen climate classes[71]. The red line indicates the average midpoint of all 347 selected chronologies. Vegetation background in **a** from open source data: Natural Earth (www.naturalearthdata.com).
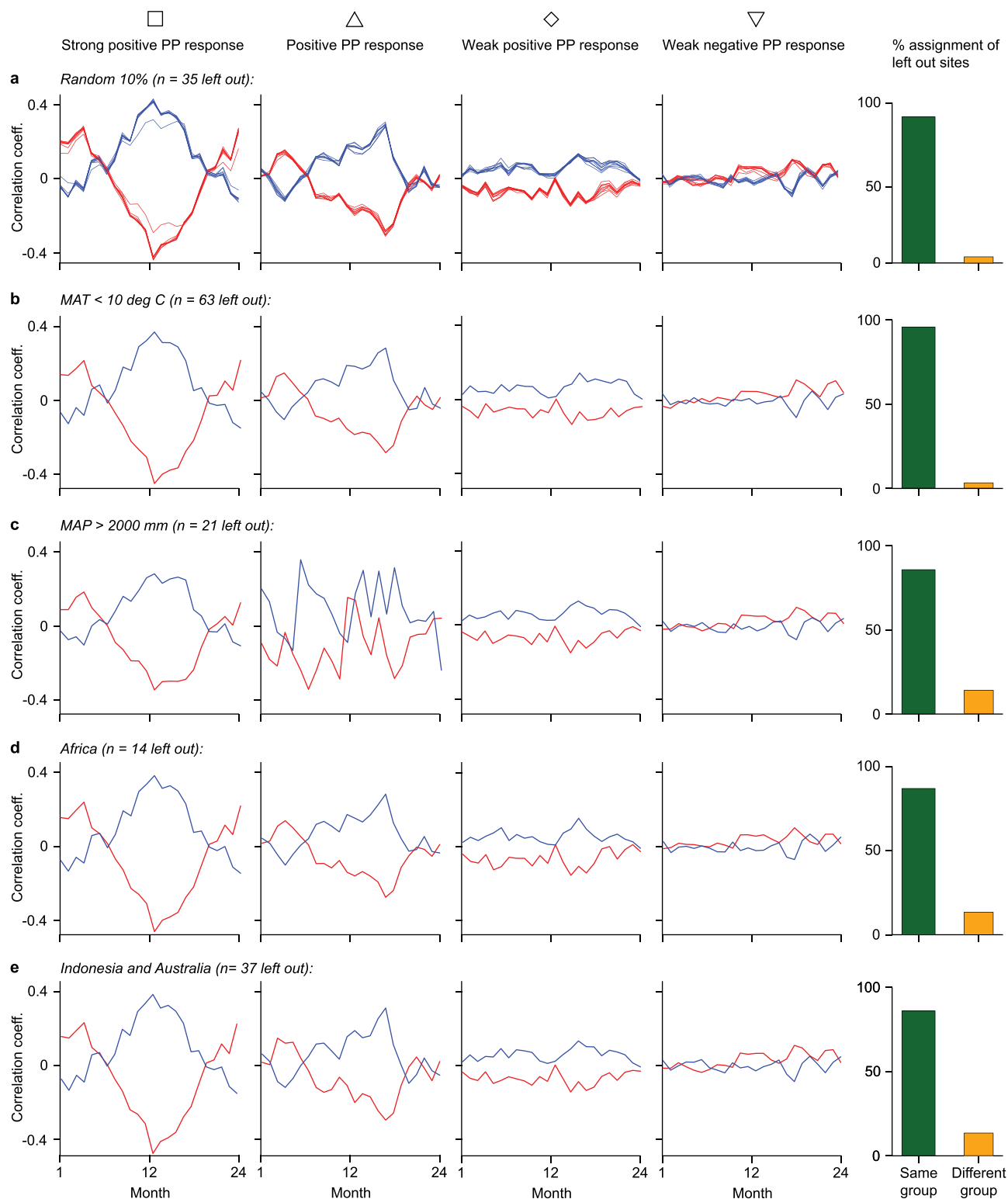
Extended Data Fig. 2 | Cross validation test of cluster analysis reveals robustness of climate response groups. Results of cross validation tests in which selections of sites were left out of the network to test robustness of climate response patterns and correctness of site assignment. Four sets of tests were conducted: removal of a random 10% of the sites (**a**, repeated 10 times), of overrepresented climates (**b**, cold sites), of underrepresented climates (**c**, wet sites) and of poorly represented regions (**d-e**). **Line graphs** per climate response group are similar to those in Fig. 2 and show mean Pearson *r* correlation coefficients of 50-year RWI series with monthly T_{max} (red) or PP (blue) for a 24-month period that covers the year of ring formation (months 1-12) and that prior to ring formation (months 13-24). **Bar graphs** show the percentage of correct and incorrect assignments of the left out sites to climate response groups.
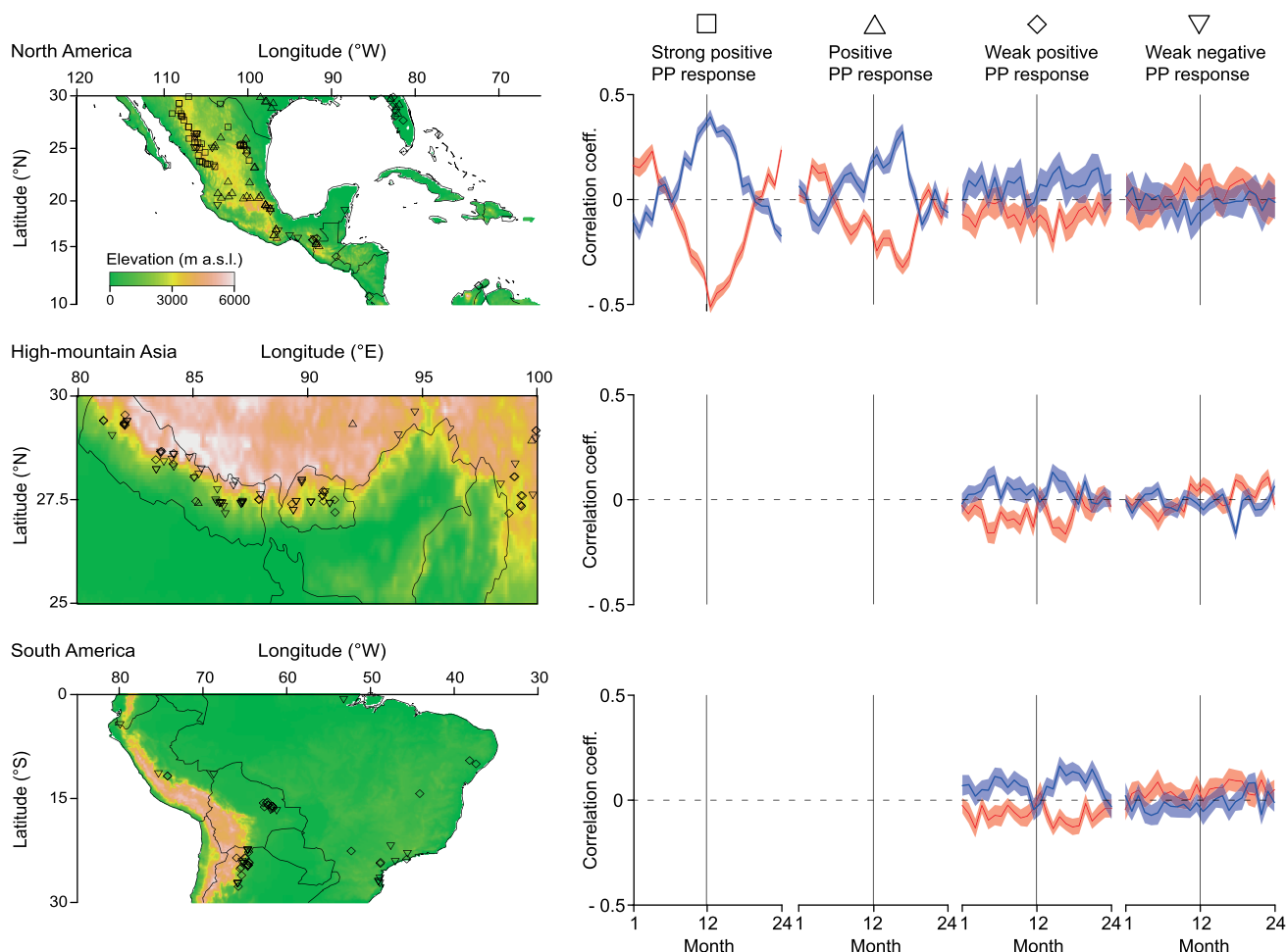
Extended Data Fig. 3 | Globally identified climate response groups are maintained at regional level. Left panels: Spatial distribution for climate response groups in well-represented sections of the network: North America ($n=119$), High-mountain Asia ($n=92$) and South America ($n=65$). In North America, climate response groups are geographically segregated and the 'Strong positive PP response' and 'Positive PP response' groups are characterized by the lowest water availability (MAP; Extended Data Table 3). Furthermore, these climate response groups differ in PP variability, whereas the groups with the weakest (positive and negative) precipitation responses differ in PP seasonality. High-mountain Asia and South America portions of the network are dominated by climate response groups with weak (positive and negative) precipitation response. As in the full network, these groups do not differ in PP variability (Extended Data Table 3). **Right panels:** Responses of ring-width index (RWI) to interannual variation in monthly T_{max} (red) and PP (blue) of four climate response groups. Correlation coefficients (Pearson r, mean and 95% confidence intervals) are shown for a 24-month period including the year prior to ring formation and that of ring formation. Elevation data for left panels from open source data: ETOPO5, NOAA (https://www.ngdc.noaa.gov/mgg/global/etopo5.HTML).
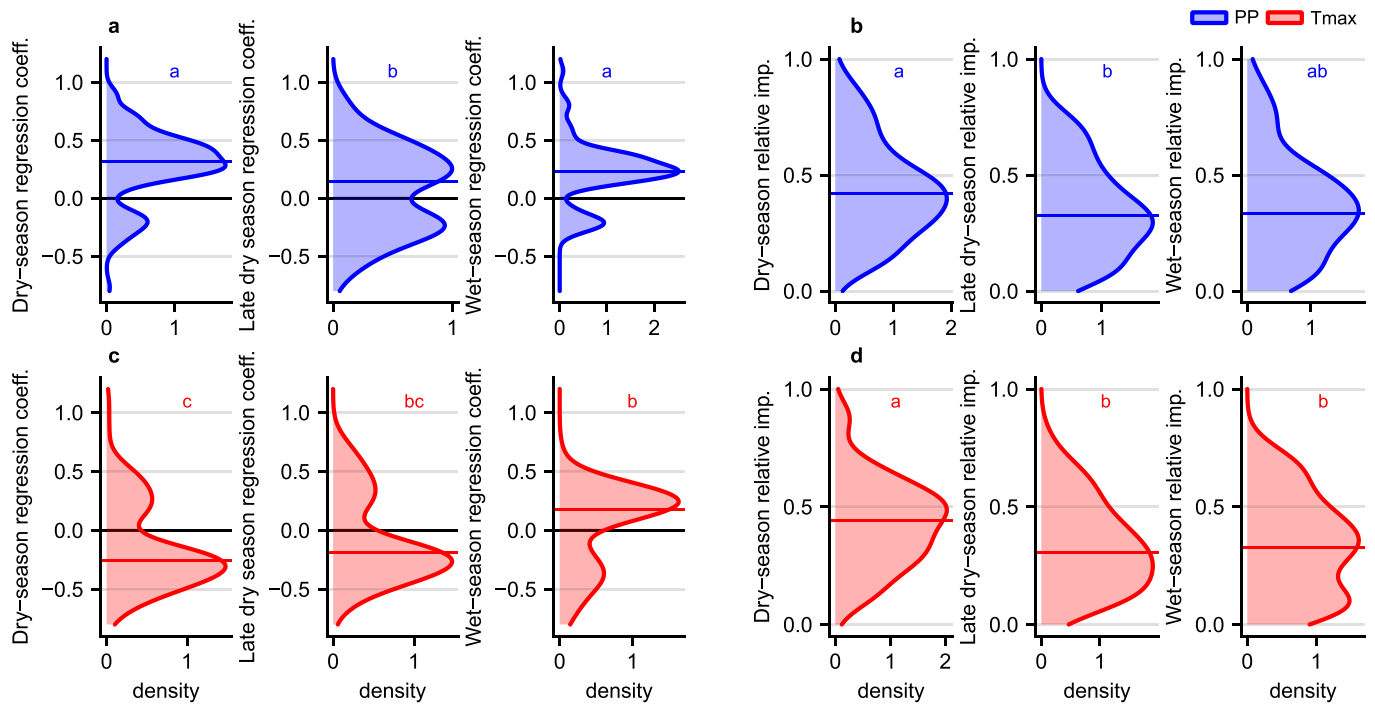
Extended Data Fig. 4 | Evaluating the roles of full vs. late dry season on tropical tree growth. a,c, Density plots of significant regression coefficients of PP (blue, **a**) and T_{max} (red, **c**) for dry season (all dry months prior to onset of wet season), late dry season (last 2 months before onset of wet season), and wet season. Density plots are based on 279 multiple regression models that included at least one significant seasonal climate effect. Letters denote significant differences between groups for either PP or T_{max} based on Wilcoxon rank test ($P < 0.05$, $n = 581$ coefficients; dry-season $n = 243$; late dry-season $n = 161$; wet-season $n = 177$). Horizonal lines represent medians. **b,d,** As panels **a** and **c** but for relative importance (only for models with >1 significant coefficient, $n = 487$).
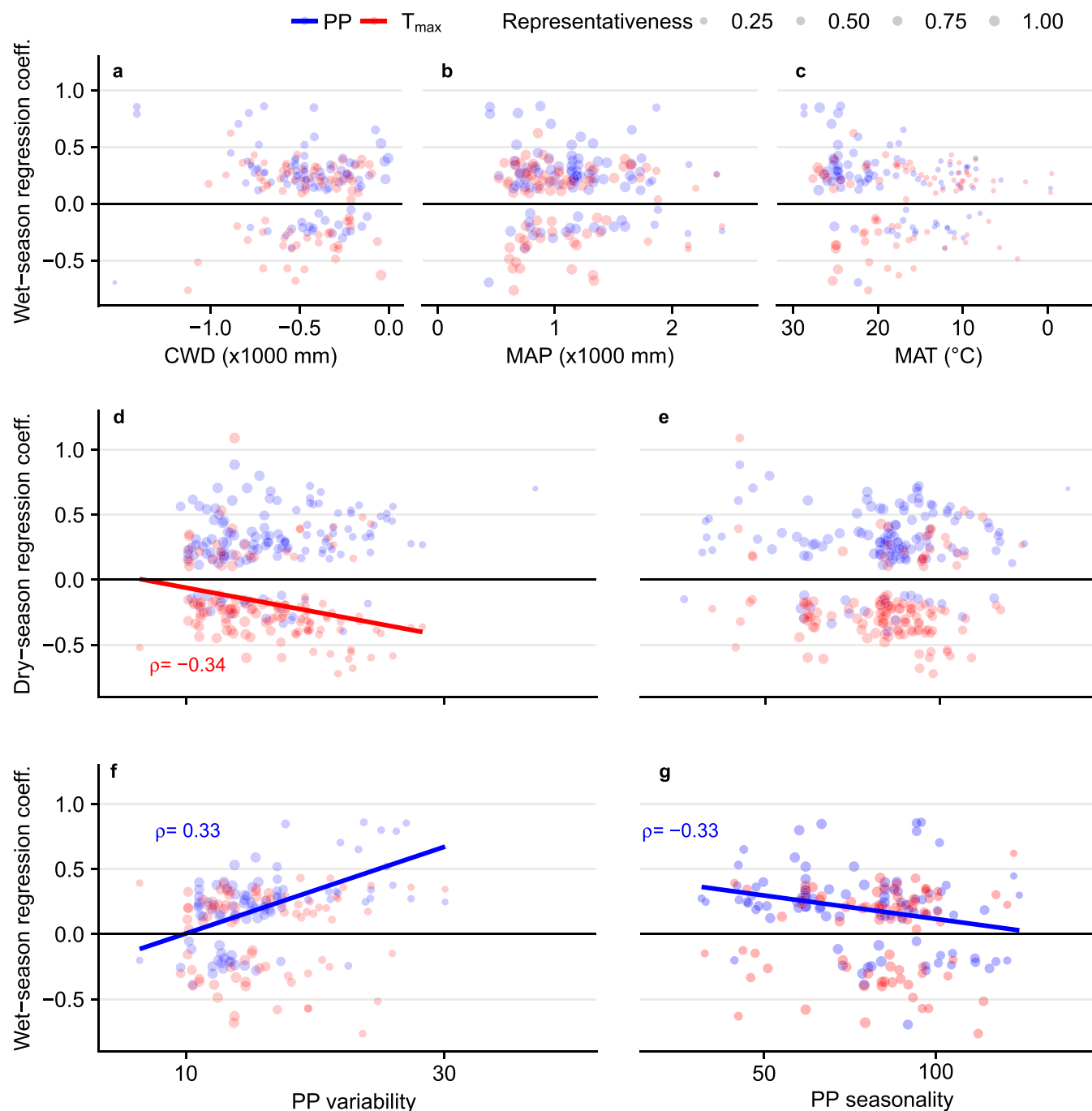
Extended Data Fig. 5 | Results of multiple regression analyses for dry and wet seasons. a-c, Association of regression coefficients for wet-season PP (blue, $n=92$) and T_{max} (red, $n=84$) with three site-specific hydroclimate variables. All hydroclimatic variables are ordered from arid (left) to humid (right). **d-g**, Association of regression coefficients for seasonal PP (blue) and T_{max} (red) with PP variability and PP seasonality. Symbol size is proportional to scaled representativeness of sites ('Density') for climate variable on X-axis (Extended Data Fig. 2). Multiple regression models are based on the most recent 50 years of each chronology. Significant correlations ($P<0.05$; Spearman rank correlation, weighted for density; Extended Data Table 4) are indicated; lines are shown for illustration only.

Extended Data Table 1 | Climate responses are robust to among-site variation in quality of gridded climate data

a. Result of Spearman's rank correlation:			Dry-season:		Wet-season:	
		PP	T_{max}	PP	T_{max}	
Non-significant ($P \geq 0.05$)		8	10	8	11	
Significantly negative ($P < 0.05$)		0	0	0	0	
Significantly positive ($P < 0.05$)		4	2	1	0	
Total number of tests (grand total = 46)		12	12	11	11	
b. Result of t-test:			'Weak positive PP response' group		'Weak negative PP response' group	
		PP	T_{max}	PP	T_{max}	
Non-significant ($P \geq 0.05$)		19	20	20	21	
Stronger correlation for sites closer to meteorological station ($P < 0.05$)		3	2	3	0	
Stronger correlation for sites further away from meteorological station ($P < 0.05$)		2	2	1	3	
Total number of tests (grand total = 96)		24	24	24	24	

a, Results of Spearman rank correlations between P-values of seasonal climate responses (Pearson correlations of RWI vs. seasonal PP and T_{max}) and distance to the nearest meteorological station (a quality proxy for gridded climate data). Rank correlations were conducted for MAP-MAT climate bins (bin size of 300 mm MAP by 3 °C MAT) that contained at least 10 sites. Only 15% of the correlations were significantly positive, suggesting a minor effect of data quality on the climate responses. **b**, Results of t-tests that compare monthly climate responses (Pearson correlation coefficients of RWI vs. monthly PP and T_{max}) for sites close to (<100 km) or further away from (>100 km) a meteorological station. Tests were conducted for the 24-months period used in SOM-clustering analysis, and for two climate response groups with >10 sites at >100 km from meteorological stations. Significantly stronger climate response for sites closer to meteorological stations were found in just 8% of the cases, and the reverse was found for a similar proportion (7%). Thus, climate growth responses were consistent for sites located close to or far away from meteorological stations.

Extended Data Table 2 | Characteristics of four climate response groups

		Climate response group			
		Strong positive PP response	Positive PP response	Weak positive PP response	Weak negative PP response
Basic information	#Chronologies	43	69	115	120
	#Countries	3	11	26	30
	% Woody vegetation area represented	3.5	47.7	67.2	46.3
	Standard deviation	0.23 [a]	0.21 [a]	0.21 [a]	0.18 [b]
	1-yr autocorrelation	-0.01 [d]	0.13 [c]	0.18 [b]	0.28 [a]
	Rbar	0.67 [a]	0.54 [b]	0.50 [c]	0.49 [c]
Geography	Latitude (° N or S)	25.4 [a]	20.1 [ab]	14.6 [b]	26.8 [a]
	Elevation (m a.s.l.)	2314 [a]	1300 [b]	1238 [b]	2685 [a]
Mean climate	MAT (°C)	11.8 [c]	20.1 [a]	19.3 [a]	16.1 [b]
	MAP (mm)	803 [b]	999 [a]	1125 [a]	1094 [a]
	CWD (mm)	-757 [c]	-524 [b]	-422 [a]	-381 [a]
	CWB (mm)	-728 [c]	-241 [b]	-244 [b]	-74 [a]
	MMWD (mm)	-127 [d]	-114 [c]	-90 [b]	-75 [a]
	# Wet months	3 [a]	4 [b]	5 [b]	4 [b]
Climate variability	PP variability (-)	20.9 [a]	16.2 [b]	14.6 [b]	13.2 [c]
	DSP variability (-)	40.7 [a]	31.7 [b]	27.4 [c]	30.5 [c]
Climate seasonality	PP seasonality (-)	90.0 [ab]	83.0 [bc]	82.9 [c]	89.5 [a]
	Precipitation Concentration Index (PCI)	14.7 [ab]	13.7 [bc]	13.7 [c]	14.8 [a]
	DSP (mm/month)	38.2 [ab]	34.9 [ab]	45.9 [a]	33.7 [b]
	DSP (mm/season)	347 [a]	263 [c]	323 [b]	254 [c]
	WSP (mm/month)	168 [NS]	163 [NS]	159 [NS]	175 [NS]
	WSP (mm/season)	515 [b]	744 [a]	786 [a]	815 [a]
ENSO responses	Pearson correlation with MEI (Multi-variate ENSO index) in current year	0.37 [a]	-0.12 [c]	-0.002 [c]	0.08 [b]
Species composition	#Species	8	22	61	50
	#Genera	4	9	37	28
	#Plant families	2	5	16	14
	#Angiosperm species	1	5	34	26
	#Angiosperm chronologies	1	22	55	40
Representa-tiveness	Latitude	0.62	0.67	0.69	0.66
	Elevation	0.06	0.34	0.31	0.16
	MAT	0.06	0.36	0.30	0.19
	MAP	0.91	0.87	0.89	0.87
	CWD	0.24	0.39	0.46	0.50
	PP variability	0.41	0.66	0.71	0.77
	PP seasonality	0.80	0.81	0.82	0.78

Shown are counts (for variables starting with '#') and medians (all other variables) per climate response group. Different letters denote climate response groups with significantly different median values in a post-hoc test (Wilcoxon rank sum test; $P < 0.05$; NS = not significant). Representativeness of geographic and climatic variables is shown as the mean of the scaled density of all sites in a climate response group for the climatic variable of interest. Rbar: mean inter-series correlation; MAT: mean annual temperature; MAP: mean annual precipitation; CWD: annual climatic water deficit; CWB: cumulative water balance; MMWD: maximum monthly water deficit; PP seasonality: seasonality of monthly precipitation; PP variability: inter annual variation in annual precipitation; DSP variability: inter annual variation in dry-season precipitation; PP seasonality: precipitation seasonality; DSP: dry-season precipitation; WSP: wet-season precipitation; ENSO: El Niño Southern Oscillation.

Extended Data Table 3 | Regional differences of climate response groups

North America		Climate response group			
		Strong positive PP response	Strong positive PP response	Strong positive PP response	Strong positive PP response
Basic info	#Chronologies	42	46	16	15
Geography	Elevation (m a.s.l.)	2332 [a]	1685 [b]	47 [c]	2500 [ab]
Mean climate	MAT (°C)	11.7 [c]	19.3 [b]	21.9 [a]	12.1 [c]
	MAP (mm)	803 [b]	856 [ab]	1255 [a]	966 [ab]
	CWD (mm)	-764 [b]	-646 [a]	-503 [b]	-549 [ab]
Climate variability	PP variability (-)	20.9 [a]	17.7 [b]	15.3 [b]	18.3 [ab]
	DSP variability (-)	40.6 [a]	30.4 [b]	30.6 [b]	39.2 [a]
Climate seasonality	PP seasonality (-)	90.1 [ab]	83.0 [ab]	61.3 [b]	95.7 [a]
	DSP (mm/month)	37.9 [NS]	35.8 [NS]	47.4 [NS]	30.9 [NS]
	WSP (mm/month)	168 [NS]	150 [NS]	169 [NS]	178 [NS]
High-mountain Asia					
Basic info	#Chronologies		3	34	58
Geography	Elevation (m a.s.l.)			3100 [b]	3284 [a]
Mean climate	MAT (°C)			9.0 [NS]	11.0 [NS]
	MAP (mm)			841 [NS]	1094 [NS]
	CWD (mm)			-273 [NS]	-310 [NS]
Climate variability	PP variability (-)			12.5 [NS]	12.6 [NS]
	DSP variability (-)			20.2 [NS]	26.7 [NS]
Climate seasonality	PP seasonality (-)			84.2 [b]	94.2 [a]
	DSP (mm/month)			32.4 [a]	34.4 [b]
	WSP (mm/month)			170 [b]	196 [a]
South America					
Basic info	#Chronologies			38	27
Geography	Elevation (m a.s.l.)			590 [NS]	1600 [NS]
Mean climate	MAT (°C)			21.8 [NS]	18.5 [NS]
	MAP (mm)			1140 [NS]	899 [NS]
	CWD (mm)			-491 [NS]	-178 [NS]
Climate variability	PP variability (-)			17.0 [NS]	16.8 [NS]
	DSP variability (-)			24.0 [b]	28.5 [a]
Climate seasonality	PP seasonality (-)			62.1 [NS]	83.8 [NS]
	DSP (mm/month)			48.2 [NS]	38.0 [NS]
	WSP (mm/month)			154.9 [NS]	151.3 [NS]

Shown are counts (for variables starting with '#') and medians (all other variables) per climate response group and for each of three well-represented regions. Different letters denote groups with significantly different median values in a post-hoc test (Wilcoxon rank sum test; $P < 0.05$; NS = not significant). Only groups represented by >10 sites were tested. MAT: mean annual temperature; MAP: mean annual precipitation; CWD: annual climatic water deficit; PP seasonality: seasonality of monthly precipitation; PP variability: inter annual variation in annual precipitation; DSP variability: inter annual variation in dry-season precipitation; PP seasonality: precipitation seasonality; DSP: dry-season precipitation; WSP: wet-season precipitation.

Extended Data Table 4 | Correlations of seasonal regression coefficients and site climate conditions

a. Dry season

		CWD		MAP		MAT		PP variability		PP seasonality	
		UW	W	UW	W	UW	W	UW	W	UW	W
PP	T_{max}	**-0.259**	**-0.232**	-0.088	-0.002	0.002	**-0.367**	**0.232**	**0.232**	0.070	0.053
	PP	**	**	NS	NS	NS	***	**	*	NS	NS
T_{max}	T_{max}	**0.425**	**0.390**	**0.317**	**0.307**	0.050	**-0.312**	**-0.341**	**-0.336**	0.015	-0.005
	PP	***	***	***	***	NS	***	***	***	NS	NS

b. Wet season

		CWD		MAP		MAT		PP variability		PP seasonality	
		UW	W	UW	W	UW	W	UW	W	UW	W
PP	T_{max}	-0.158	-0.077	-0.049	-0.019	**0.362**	0.181	**0.467**	**0.332**	**-0.273**	**-0.328**
	PP	NS	NS	NS	NS	***	NS	***	**	**	**
T_{max}	T_{max}	0.027	0.066	0.046	0.102	-0.126	0.110	0.104	0.039	-0.010	-0.047
	PP	NS	NS	NS	NS	NS	NS	NS	NS	NS	NS

Results of unweighted (UW) and weighted (W) Spearman rank correlations between site climate variables (CWD, MAP, MAT, PP variability, and PP seasonality) and significant regression coefficients for PP and T_{max} during dry (**a**) or wet (**b**) season. The weighted correlation analysis accounts for the under- and over-representation of climatic conditions in our network by weighing data points by the relative density of tropical woody vegetation for the value of the climate variable under consideration (green lines in Extended Data Fig. 2). A total of 438 significant regression coefficients were obtained from 260 multiple regression models that contained at least one significant effect (out of the 347 models conducted for all chronologies). Significance levels: *: $0.01 < P < 0.05$; **: $0.001 < P < 0.01$; ***: $P < 0.001$. Sample sizes dry season: PP, n=130; T_{max}, n=132; wet season: PP, n=92; T_{max}, n=84.

Extended Data Table 5 | Predicted warming at network sites

Predicted increase in:	SSP	2021-2040	2041-2060	2061-2080	2081-2100
T_{max} (°C)	370	1.32 ± 1.24	2.21 ± 1.27	3.21 ± 1.31	4.35 ± 1.37
	585	1.49 ± 1.25	2.58 ± 1.26	3.95 ± 1.32	5.59 ± 1.41
T_{min} (°C)	370	1.25 ± 1.2	2.11 ± 1.23	3.08 ± 1.26	4.18 ± 1.33
	585	1.37 ± 1.21	2.44 ± 1.23	3.77 ± 1.3	5.36 ± 1.42
T_{mean} (°C)	370	1.29 ± 1.14	2.16 ± 1.17	3.15 ± 1.2	4.27 ± 1.26
	585	1.43 ± 1.14	2.51 ± 1.16	3.86 ± 1.22	5.47 ± 1.32

Predicted maximum (T_{max}), minimum (T_{min}), and mean (T_{mean} = T_{max} - T_{min}) warming, averaged across all 347 sites until 2100, and relative to 1970-2000 values. For each site, predictions of 9 GCMs were averaged, and then site-specific values were averaged, and their SD calculated. Predictions are shown for two Shared Socio-economic Pathways (SSPs).